VŠB – Technická univerzita Ostrava

Univerzitní studijní programy

Preparation of titanium dioxide using titanylsulphate and its characterization.

Příprava oxidu titaničitého z titanylsulfátu a jeho charakterizace.

Bc. Jaroslav Lang

Vedoucí diplomové práce: doc. Ing. Vlastimil Matějka, Ph.D.

Datum odevzdání: 15.05.2013

VŠB - Technical University of Ostrava
University Study Programmes
CNT - Nanotechnology Centre

Diploma Thesis Assignment

Student:	**Bc. Jaroslav Lang**
Study Programme:	N3942 Nanotechnology
Study Branch:	3942T001 Nanotechnology
Title:	Příprava oxidu titaničitého z titanylsulfátu a jeho charakterizace Preparation of titanium dioxide using titanylsulphate and its characterization

Description:

Cílem práce je připravit a následně charakterizovat oxid titaničitý s využitím titanylsulfátu jako prekurzoru.

Teoretická část zahrnuje vypracování literární rešerše v těchto oblastech:
1. Oxid titaničitý (vlastnosti, využití).
2. Metody přípravy oxidu titaničitého z titanylsulfátu.
3. Vybrané metody charakterizace oxidu titaničitého (RTG difrakční analýza, měrný povrch a porosita, mikroskopické techniky, termická analýza, stanovení fotokatalytické aktivity).

Praktická část zahrnuje provedení následujících experimentů:
1. Příprava oxidu titaničitého z roztoku titanylsulfátu včetně přípravy výchozího roztoku.
2. Úprava připravených vzorků oxidu titaničitého (snížení obsahu vázaných sulfátů neutralizací a vymytím, kalcinace).
3. Charakterizace připraveného oxidu titaničitého pomocí RTG difrakční analýzy, termické analýzy, stanovení fotokatalytické aktivity vybraných vzorků, SEM, měrný povrch a porosita.

The aim of the master thesis is preparation and characterization of titanium dioxide prepared using titanylsulphate as a precursor.

The theoretical part comprises elaboration of literature search covering following areas:
1. Titanium dioxide (properties, utilization).
2. The methods for the preparation of titanium dioxide using titanylsulphate.
3. Selected methods for characterization of the titanium dioxide (X-ray diffraction method, specific surface area and porosity, microscopy techniques, thermal analysis, evaluation of photocatalytic activity).

Experimental part comprises:
1. Preparation of titanium dioxide sol using titanylsulphate, icluding preparation of the initial solution.
2. Treatment of the prepared titanium dioxide with the aim of the sulphate content minimalization using neutralisation, washing and calcination.
3. Charaterization of the prepared titanium dioxide using X-ray diffraction method, thermal analysis, characterization of the photocatalytical activity of the selected samples, scanning electron microscopy, specific surface area and porosity.

References:

1. CARP, O.; HUISHMAN, C.; KELLER, A. Photoinduced reactivity of titanium dioxide. Progress in Solid State Chemistry, 2004, Vol. 32, pp. 33-177.
2. GATEHOUSE, B. M.; PLATTS, S. N.; WILLIAMS, T. B. Structure of anhydrous titanyl sulfate, titanyl sulfate monohydrate and prediction of a new structure. Acta Crystallographica Section B, 1993, Vol. B49, pp. 428-435.
3. SIVAKUMAR, S.; KRISHNA PILLAI P.; MUKUNDAN, P.; WARRIER, K. G. K. Sol-gel synthesis of nanosized anatase from titanyl sulfate. Materials Letters, 2002, Vol. 57, pp. 330-335.

Extent and terms of a thesis are specified in directions for its elaboration that are opened to the public on the web sites of the faculty.

Supervisor: **Ing. Vlastimil Matějka, Ph.D.**

Date of issue: 16. 11. 2012

Date of submission: 15. 05. 2013

prof. Ing. Jaromír Pištora, CSc.
Head of Department

VYSOKÁ ŠKOLA BÁŇSKÁ - TECHNICKÁ UNIVERZITA OSTRAVA
UNIVERZITNÍ STUDIJNÍ PROGRAMY

prof. Ing. Petr Noskievič, CSc.
Vice-rector for Study Affairs

PROHLÁŠENÍ

- Byl(a) jsem seznámen s tím, že na moji diplomovou práci se plně vztahuje zákon č.121/2000 Sb. – autorský zákon, zejména § 35 – využití díla v rámci občanských a náboženských obřadů, v rámci školních představení a využití díla školního a § 60 – školní dílo.
- Beru na vědomí, že Vysoká škola báňská – Technická univerzita Ostrava (dale jen VŠB –TUO) má právo nevýdělečně, ke své vnitřní potřebě, diplomovou práci užít (§ 35 odst. 3).
- Souhlasím s tím, že jeden výtisk diplomové práce bude uložen v Ústřední knihovně VŠB-TUO k prezentačnímu nahlédnutí a jeden výtisk bude uložen u vedoucího diplomové práce. Souhlasím s tím, že údaje o diplomové práci, obsažené v Záznamu o závěrečné práci, umístěném v příloze mé diplomové práce, budou zveřejněny v informačním systému VŠB-TUO.
- Bylo sjednáno, že s VŠB-TUO, v případě zájmu z její strany, uzavřu licenční smlouvu s oprávněním užít dílo v rozsahu § 12 odst. 4 autorského zákona.
- Bylo sjednáno, že užít své dílo – diplomovou práci nebo poskytnout licenci k jejímu využití mohu jen se souhlasem VŠB-TUO, která je oprávněna v takovém případě ode mne požadovat přiměřený příspěvek na úhradu nákladů, které byly VŠB-TUO na vytvoření díla vynaloženy (až do jejich skutečné výše).
- Místopřísežně prohlašuji, žě celou diplomovou práci včetně příloh, jsem vypracoval(a) samostatně a uvedl(a) jsem všechny použité podklady a literaturu.

V Ostravě dne 15.5.2013 ……..

podpis

ANOTACE DIPLOMOVÉ PRÁCE

LANG, J. *Příprava oxidu titaničitého z titanylsulfátu a jeho charakterizace: diplomová práce.* Ostrava: VŠB – Technická univerzita Ostrava, Univerzitní studijní programy, 2013, 61 s. Vedoucí práce: Matějka, V.

Diplomová práce se zabývá přípravou a charakterizací fotoaktivního oxidu titaničitého. Nanostrukturovaný oxid titaničitý je významným fotokatalyzátorem využívaným v mnoha odvětvích od čištění vody až po samočistící povrchy. Tato diplomová práce se zabývá přípravou oxidu titaničitého sulfátovou metodou. Jako prekurzor titanu byl použit titanyl sulfát, vzorky oxidu titaničitého byly připraveny ve formě prášku. Připravené vzorky byly charakterizovány vybranými metodami chemické a fázové analýzy, morfologie vzorků byla studována pomocí mikroskopických technik. U připravených materiálů byla testována jejich fotodegradační aktivita.

Klíčová slova: fotokatalyzátor, oxid titaničitý, titanyl sulfát, sulfátová metoda

ANNOTATION OF DIPLOMA THESIS

LANG, J. *Preparation of titanium dioxide using titanylsulphate and its characterization: Diploma Thesis.* Ostrava: VŠB – Technical University of Ostrava, University Study Programmes, 2013, 61 p. Thesis supervisor: Matějka, V.

The diploma thesis focuses on the preparation and characterization of photocatalytic active titanium dioxide. Nanostructured titanium dioxide is an outstanding photocatalyst finding a variety of applications ranging from the water treatment to the preparation of the self-cleaning surfaces. This diploma thesis focuses on the preparation of the titanium dioxide using the sulphate method. Titanyl sulphate was used as a titanium precursor and the samples of titanium dioxide were prepared in the form of powder. The prepared samples were characterized using methods of chemical and phase analysis. The morphology of the samples was studied using microscopy techniques. The prepared samples were examined for evaluation of their photodegradation activity.

Key words: photocatalyst, titanium dioxide, titanyl sulphate, sulphate method

List of abbreviations and symbols

Ads = adsorbed

BET = Brunauer–Emmett–Teller theory

BSE = backscattered electrons

CAS = chemical abstract service

CB = conductive band

CIE = color space defined by International Commission on Illumination

CIELAB = color space devised from CIE color space

ΔG^0 = Gibbs free energy

Demi = demineralized

DLVO = Deryagin, Landau, Verwey and Overbeek theory

DSC = differential scanning calorimetry

EDX = Energy-dispersive X-ray spectroscopy

Eg = band gap energy

HTD = hydrated titanium dioxide

IUPAC = International Union of Pure and Applied Chemistry

IR = infra red

Lc = crystallite size

Min. = minutes

Ox = oxidized

pH = hydrogen ion concentration

Red = reduced

S_{BET} = specific surface area calculated from Brunauer–Emmett–Teller theory

SE = secondary electrons

SEM = scanning electron microscopy

SSA = specific surface area

TA = thermal analysis

TEM = Transmission electron microscopy

TG = thermogravimetric analysis

UV = ultraviolet

VB = valence band

V_{NET} = net pore volume

XRD = X-ray diffraction

CONTENT

1 Introduction

Nanomaterials quickly find their way to products in our everyday life. What are those nanomaterials that are marketed to us in so many products? Nanomaterial is defined as a material whose size does not overcome 100 nanometers (1 nm = 1.10^{-9}m) at least in one direction [1]. The dispersions of nanoparticles are studied in colloid chemistry.

Nanomaterials are nothing alien to the human and nature. Natural nanoparticles can be found in volcanic ash. Carbon nanoparticles as a product of combustion are found in soot, even living creatures contain nanoparticles – cell organelles can be regarded as nanodevices and also viruses meets the criteria for nanoparticles. Nanoparticles play role in such vital processes like weather where they serve as nucleation centers for water to condense on and thus creating rain drops. People encounter nanomaterials daily even without knowing it.

Large range of products utilizing nanoparticles from cosmetics, clothing and protective coatings of sport instruments can be find on nowadays market as shown in Fig. 1. Nanomaterials are used because they exhibit useful new properties which are not observable in their bulk form, whereas titanium dioxide is a good representative of that. Its bulk form is used in pigment industry where it has a major share in white pigment production. Its nanosized form presents properties like photoactivity and superhydrophilicity, which can be used for creation of antibacterial surfaces, antifogging glasses, self-cleaning surfaces and solar cells [1].

Fig. 1 Variety of products utilizing nanomaterials [1].

The combination of properties of bulk and nano forms of materials could result in material with great ecological impact. By application of thin layer of paint consisting of

nanosized TiO_2 white colored surface showing photodegradation, antibacterial, self-cleaning properties can be obtained. That means, while fulfilling its aesthetical role as a white pigment, titanium dioxide would also reduce the air pollution utilizing its photocatalytic properties or save maintenance money because of its self cleaning feature. With the continuation of widespread use of white pigments on light exposed surfaces and walls it presents substantial way of reducing air pollution.

2 Theory

This part of the thesis provides brief insight to origin and factors affecting the properties of TiO_2 and to the process of TiO_2 preparation.

2.1 Titanium dioxide

TiO_2 is a compound of titanium and oxygen. In nature it occurs in three crystallographic phases (anatase - tetragonal, rutile - tetragonal, brookite - orthorhombic) and although other phases do exists they are not very that common. The structure of anatase crystallographic phase is shown in Fig. 2. Titanium dioxide has CAS registry number: 13463-67-7 [2].

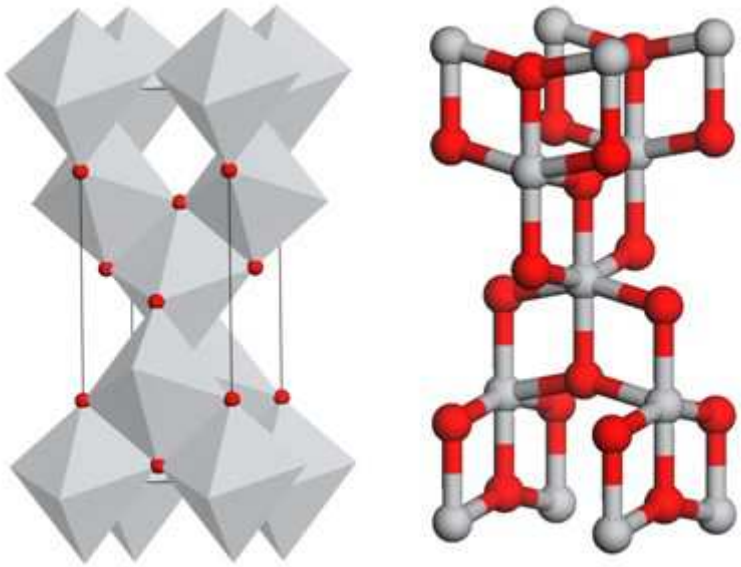

Fig. 2 Anatase crystallographic phase structure [3].

Titanium dioxide is a semiconductor and semiconductors can be characterized by their band gap. The band gap energy (Eg) is specific for each crystallographic phase of TiO_2. The anatase phase has indirect band gap Eg = 3.2 eV and rutile phase direct band gap Eg = 3.02 eV [4, 5]. The band gap and its meaning for the photocatalytic properties of TiO_2 will be further explained in the chapter 2.2 “Photoactivity”.

Until the rediscovery of photocatalytic properties of the anatase phase by Fujishima in 1970s the main application of TiO_2 was in pigment industry.

The rutile phase is used in pigment industry as a white pigment for its optical properties like opacity, high brightness and high refractive index. TiO_2 is also recognized as non-toxic and substitutes previously used white pigment Anglesite which contains highly toxic lead

(Lead(II) sulphate - $PbSO_4$). Excellent pigmentary properties of TiO_2 are followed with good processing properties like dispersibility and weather resistance.

One of the main natural sources of economically affordable TiO_2 is mineral ilmenite (iron titanium oxide - $FeTiO_3$). It got its name after mountains Ilmen in Chelyabinsk Oblast', Southern Urals, Urals Region, Russia. The biggest producers of ilmenite are USA, Norway, Canada, Russia and India [6-8]. Other significant sources of TiO_2 are leucoxene which is a weathering product of ilmenite, titanium slag and synthetic rutile [9].

2.2 Photoactivity

Photocatalysts are generally semiconductors, at which the transition of electron from valence band (VB) to conductive band (CB) is caused by photoexcitation by the photon with energy higher than the energy of the band gap (Eg). The Eg is situated between VB and CB as shown in Fig. 3.

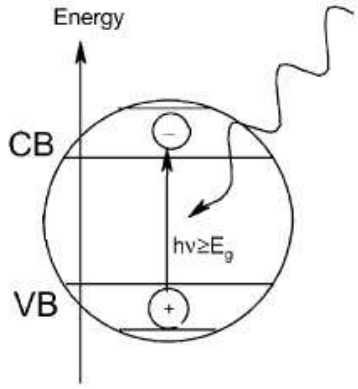

Fig. 3 Photoexcitation of electron in semiconductor [4].

The band gap is amount of energy needed for excitation of electron from valence band to conductive band and also an energy range in a solid where no electron states can exist [4]. The energy can be supplied by electromagnetic irradiation with sufficient wavelength. The relation between energy and wavelength is given by equation (1).

$$E = \frac{hc}{\lambda} \tag{1}$$

Where E is energy (eV), h is Planck constant (eVs), c is speed of light (m/s), λ is wavelength (nm). For TiO_2 the band gap energy is 3.2 eV for anatase and 3.02 eV for rutile, which corresponds to the energy of the photon with wavelength of 387 nm and 410 nm respectively [4].

The transition of the electron from VB to CB can be direct (the momentum of the electron is conserved) or indirect (for the transition to occur the electron has to change a momentum and for that it requires interaction with lattice vibration called a phonon).

Next to the band gap energy, the ability of semiconductor to transfer photoinduced electron to an adsorbed particle which is determined by the band energy positions of the semiconductor and the redox potential of adsorbed compounds is necessary for the progress of photocatalytic reactions.

The energy level at the bottom of the conduction band corresponds to the reduction potential of photoinduced electrons. The energy level at the top of the valence band corresponds to the oxidation ability of photoinduced holes. Both of these values determine the reduction and oxidation ability of the system [4]. The band positions: top of the valence band and bottom of the conductive band of several semiconductors and selected redox potentials are schematically shown in Fig. 4.

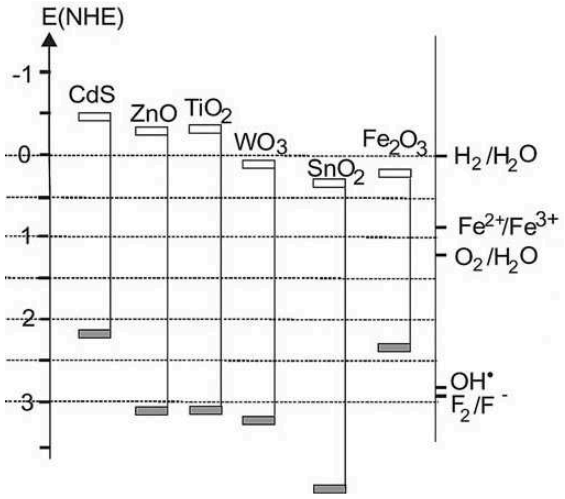

Fig. 4 The band positions of several semiconductors together with chosen redox potentials. Where E(NHE) is energy of normal hydrogen electrode, darker rectangles represents the top of the valence band, the lighter rectangles represents the bottom of the conductive band [4].

The lack of continuum of interband states of semiconductors in comparison to metals, prolongs the recombination time of electron-hole pair. The recombination time is affected by the nature of the electron transition. The indirect transition requires also a presence of phonon. The longer recombination time enables diffusion of electrons and holes to catalyst's (photocatalytic active semiconductor's) surface and to initiate redox reaction [4].

2.2.1 Photoinduced reactions on a semiconductor particle

The electron-hole pair is generated after absorption of photon with sufficient energy. The generated electron-hole pair is responsible for oxidation and reduction reactions that take

place on the surface of the semiconductor particle. The oxidation and reduction reactions together with the electron-hole recombination take place at the same time, but with different reaction speeds [4]. The scheme of photoinduced reactions on the semiconductor particle is shown in Fig. 5.

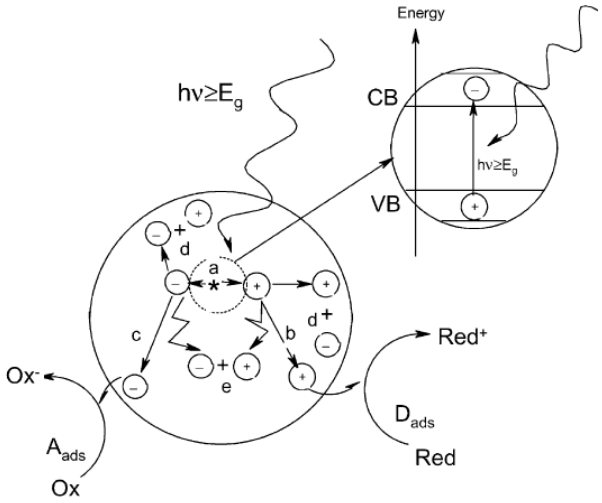

Fig. 5 Scheme of photoinduced reactions on the semiconductor particle. A- Acceptor, D- donor, $_{ads}$- adsorbed, hν - photon energy, Eg- band gap energy, a) generation of electron-hole pair, b) oxidation reaction, c) reduction reaction, d) surface electron–hole recombination, e) bulk electron-hole recombination [4].

The photoinduced reactions shown in Fig. 5 correspond to the reactions on the surface of TiO_2 particle and are most often expressed by the following scheme [4]:

a) $TiO_2 + h\nu \rightarrow TiO_2\,(e^- + h^+)$ generation of electron-hole pair

b) $e^- + M^{n+} \rightarrow M^{(n-1)+}$ reduction reaction of metal cation

or $e^- + O_2\,(ads) \rightarrow O_2^{\bullet -}$ oxygen radical generation from adsorbed O_2

c) $h^+ + H_2O \rightarrow HO\bullet + H^+$ oxidation of adsorbed water

(hν - photon energy, M^{n+}- metal ion, h^+- hole, e^-- electron)

2.2.2 Photosynthesis vs. photodegradation

The scheme of photocatalyzed reaction (1) is shown below:

$$(\mathrm{Ox}_1)_{\mathrm{ads}} + (\mathrm{Red}_2)_{\mathrm{ads}} \xrightarrow[h\nu > E_g]{semiconductor} \mathrm{Red}_1 + \mathrm{Ox}_2 \qquad (1)$$

In most photosynthesis reactions involving TiO_2, ΔG^0 is negative ($\Delta G^0 < 0$) and the reactions are photocatalytic rather than photosynthetic [4].

Almost every functional group with non bonded electron pair or with π-conjugation is prone to oxidation by TiO_2. Reductive transformation of organic compound is possible under certain experimental conditions (absence of oxygen and source of proton). The reductive transformation is usually less efficient than the oxidative one. There are two reasons:

1. The reducing power of a conduction band electron is significantly lower than the oxidizing power of a valence band hole.
2. The most reducible substrates cannot kinetically compete with oxygen in trapping photogenerated conduction band electrons.

Thus, the main research focus is on the photodegradation of compounds rather than their photosynthesis [4].

2.2.3 Photodegradation of organic compound

As mentioned above, the reductive transformation of organic compounds is usually less efficient than the oxidative one. The photodegradation of organic compound proceeds by its direct oxidation by hole (h^+) and indirect oxidation by hydroxyl radical HO•.

The photodegradation of the organic compound proceeds according to these reactions:

$h^+ + R \rightarrow R^{\bullet}$ direct oxidation

$HO\bullet + R\text{-}H \rightarrow R\bullet + H_2O$ indirect oxidation of organic compound R [10].

The photodegradation of organic compound can indirectly proceed by other activated oxygen species e.g. O_2^-, HOO^-, HOOH, HOO^-, HO^-, depending on the reaction conditions. The organic compounds can be degraded to basic inorganic compounds such as water, carbon dioxide and mineral acid [4].

There are three approaches to enhance photocatalytic activity:

1. **Band gap tuning** - by altering chemical composition of photocatalyst, ergo electronic structure, influencing which part of the electromagnetic spectra will be able to excite

electron in photocatalyst. It is performed by addition of sensitizers and through doping (noble metals, transition metals, lanthanide metals, nonmetals, etc.) [11, 12].

2. **Reducing charge carrier recombination** - decreasing the size of the photocatalyst particles reduces the distance which charge carriers (electrons and holes) must travel to the surface and enables utilization of their charge (energy) before their recombination. The reduction of the size of photocatalyst particle is accomplished during the synthesis of the catalyst [11].
3. **Modifying surface chemical reactions** - by altering the surface of the photocatalysts by supporting materials which promote the forward reaction and quickening the absorbance of reactants and their desorption. It is achieved by using high surface area support structures and by modifying the surface chemical composition [11].

2.2.4 Parameters affecting photodegradation process

The photodegradation process can be affected by several ways. These approaches are realized by careful adjustment of parameters like photocatalyst dosage, UV light intensity, concentration and nature of the pollutant, temperature, oxygen concentration, pH, humidity for photodegradation reactions in gaseous phases and others which can significantly affects photodegradation rate [4].

The main factors influencing the photodegradation process are mainly:

Dosage - With higher dosage of the photocatalyst the total surface area grows and therefore more active sites are available. On the other hand In the case of overdose the photocatalytic particles may shield each other from the illumination and prevent efficient use of photons [13, 14].

UV light intensity - The reaction order is dependent on the intensity of used light. The borderline intensity is 25 mW/cm^2. The first order regime is for intensities up to 25 mW/cm^2, half order regime is for intensities above the 25 mW/cm^2 borderline. With increasing light intensity more electron-hole pairs are generated and the rate of photodegradation is higher [14].

Concentration and nature of pollutant - The photocatalyst has limited amount of active sites and in the situation of excess amount of pollutant the active sites are saturated and the photodegradation reactions have constant rate [4].

Temperature - The photocatalytic oxidation is not much affected by minor temperature changes (the energy to excite electron from the valence to conductive band is greater than the

thermal energy available at the room temperature). However, the temperature affects desorption time of the pollutant, with higher temperature the desorption time is shorter [4].

Oxygen concentration - The dissolved molecular oxygen is electrophylic and reduces electron-hole recombination. However at high concentration of the oxygen the surface of TiO_2 becomes intensively hydroxylated by OH groups which inhibit the adsorption of the pollutant [4].

pH - The pH affects surface charge of the photocatalyst, size of agglomerates, ionization and speciation of organic pollutant. Electrostatic interactions between photocatalyst, pollutant, solvent, species created during photocatalytic process and the whole process of the photocatalytic oxidation is greatly dependent on pH.

It was reported that the positive charge on the surface of TiO_2 photocatalyst increases with the decrease in pH. The positive holes are determining oxidative species at lower pH and hydroxyl radicals are predominant at neutral and high pH [4, 14].

Humidity for photodegradation reactions in gaseous phases - The water plays important role in the constant production of hydroxyl radicals for catalytic activity, as can be seen in above mentioned reaction c) $h^+ + H_2O \rightarrow HO\bullet + H^+$ [4].

High-surface area - photocatalysts with high specific surface area show increased photocatalytic activity due to the high number of active sites available on the surface. This is best utilized in powder materials [11].

2.3 Colloids

What are the colloids? Colloids are systems with colloid dispersion, that means systems with size of the dispersed particles between 5 nm to 1μm [15].

Colloid dispersed systems can be divided according to affinity between dispersed phase and dispersion medium [15]:

Lyophobic dispersions – in lyophobic systems (from greek *lyos* - liquid and *phobos* - to hate) dispersed phase is insoluble and has no affinity to dispersion medium. Lyophobic dispersions are typical heterogeneous systems (will be discussed further in the text).

Lyophilic dispersions – in lyophilic systems (from greek *filo* - to love) dispersed phase has affinity to dispersion medium. Lyophilic dispersions are macromolecular solutions which displays some features typical for colloid dispersion.

Associative colloids - colloids where dispersed particles are created by reversible association of amphiphilic molecules into organized clusters called micelles. Forming of the

micelles is possible due to the composition of the amphiphilic molecules - one part of the molecule has great affinity towards the dispersion phase - “tail” and the other part of the molecule is insoluble in the dispersion phase ”head”. The - “heads” are in the center of the micelle and the “tails” are facing outwards from the center [15].

2.3.1 Lyophobic colloid

Colloid particles are usually not isolated molecules but rather clusters of molecules. Thanks to phase boundary separating the phases colloid system can be classified as heterogeneous system even though all involved phases have the same physical state. The boundary can exist when one of the phases is insoluble or very little soluble. The classification of the heterogeneous systems is shown in Tab. 1 [15].

Tab. 1 Classification of the heterogenous dispersion systems according to the physical state.

Medium	**dispersed phase**	**dispersion system**	
		Colloid d.	**Coarse d.**
Gas	gas	---	---
	liquid	liquid aerosol*	mist
	solid	solid aerosol*	smoke
Liquid	gas	foam	foam
	liquid	emulsion	emulsion
	solid	lyosol*	suspension
Solid	gas	solid foams	minerals with encapsulated gas
	liquid	gel	minerals with encapsulated droplets
	solid	solid sol*	eutectics

* In colloid chemistry it is customary to describe all colloid dispersed systems as *sols* (hence aerosol, lyosol, …) [16].

Following features are specific for colloid dispersions [15]:

- Colloid particles are not visible using optical microscopy but can be detected by ultramicroscopy (utilizing Tyndall effect- light scatterred on small (colloid size) particles dispersed in medium).

- Opalescence - a type of dichroism when the color of the material appears to be yellowish-red in transmitted light and blue in the scattered light perpendicular to the transmitted light.
- Particles are too small to be filtered using filtration paper but too big for membranes.
- In comparison to molecular dispersion the Brownian movement of the particles is smaller.
- Slow diffusion and sedimentation.
- Small osmotic pressure (colligative property- depends on the number of particles).
- Stability issues - kinetic stability but aggregate lability. Kinetic stability refers to small changes in distribution of particle concentration in gravitation field - slow sedimentation. Aggregate lability refers to liability of colloids to change their degree of dispersion.

Colloid features are not restricted to inorganic compounds, organic compounds creates colloids too, e.g. milk, blood [15].

2.3.2 Preparation of lyophobic colloid

There are two approaches to the preparation of lyophobic colloids. One way is the dispersion of larger particles into smaller ones through methods like milling and ultrasonication. The other method is condensation of molecules into larger particles [15].

The condensation method - This approach is based on the formation of the nucleation centers from the solution. If the starting solution is oversaturated the spontaneous nucleation occurs. Nucleation can be stimulated by the inoculation of the saturated solution by the introduction of nucleation centers. Condensation method is affected by nucleation and growth of nuclei. Oversaturation of the starting solution can be induced by the manipulation of physico-chemical conditions like temperature, pressure, solvent composition, or it can be achieved by the chemical reaction of the dissolved compounds. Dispersion system can be prepared by the means of various chemical reactions (oxidation, reduction, precipitation, hydrolysis, etc.) whose products are less soluble than precursors [15].

2.3.3 Particle growth

Due to the high degree of dispersion in colloid systems the particles have large surface area which is significant for adsorption and other surface phenomena unlike in the molecular dispersions or coarse dispersions where the volume properties are prevalent.

The large surface area of the phase boundary is associated with great interphase boundary energy and grows with the degree of dispersity. Therefore colloid systems spontaneously decrease their degree of dispersity through one of these methods [15]:

Ostwald ripening – small particles have greater surface curvature than larger particles (surface curvature has relation to overall surface of the dispersed phase that is related to the surface energy). The diffusion of small particles to larger ones leads to lowering of the surface energy in the system. Speed of the process depends on the volatility of the medium, diffusion coefficient and surface tension [15]. The process of Ostwald ripening is illustrated in Fig. 6.

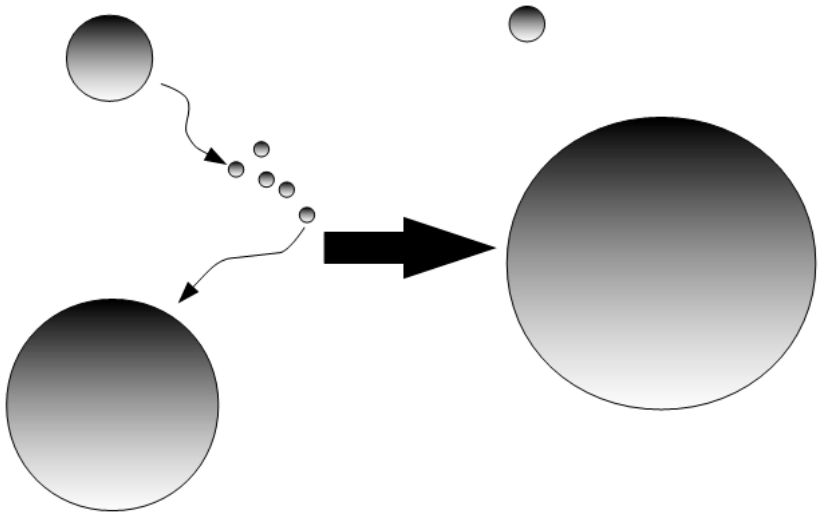

Fig. 6 The Ostwald ripening mechanism of particle growth.

Aggregation – this mechanism is more common than Ostwald ripening and generally has faster mechanism. Dispersed particles link together and form larger aggregates. Formation of aggregates is possible thanks to attractive Van der Waals forces which take place between the dispersed particles [15]. The process of aggregation is depicted in Fig. 7.

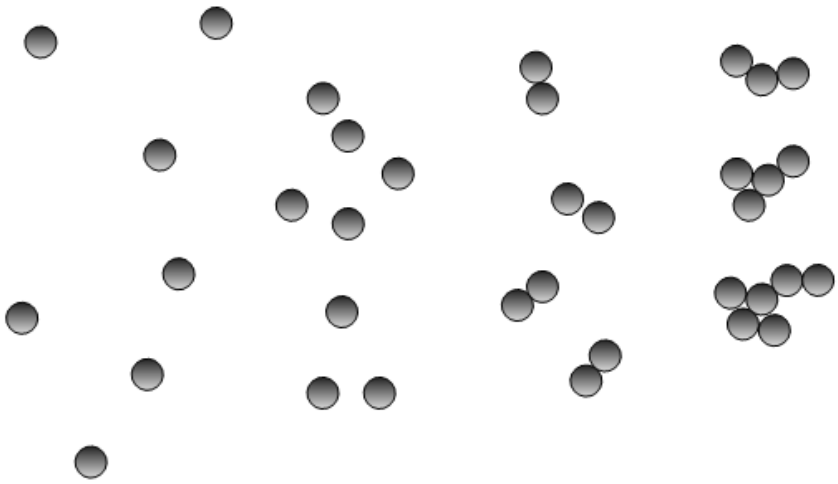

Fig. 7 The mechanism of aggregates formation.

The Van der Waals forces includes: Keesom force - interaction between two dipoles, Debye force - interaction between permanent dipole and induced dipole, London dispersion force - interaction between two induced dipoles [15].

Flocculation is a type of aggregation where particles are not so strongly bound together and thus the flocculation is reversible, the reverse process where larger aggregates are dispersed into smaller particles is called peptization [15].

Coagulation on the other hand is a type of aggregation that leads to strongly bound particles in aggregates. Coagulation is irreversible process. If the nature of the aggregates is not known the process of their formation is usually described as coagulation [15].

2.3.4 Stabilization of the colloids suspensions

The way of preventing aggregation of the particles into agglomerates with sizes larger than colloid dispersion is achieved by the stabilization - electrostatic or steric [15].

Electrostatic stabilization –is based on the phenomenon that two particles with same charge repel each other. This phenomenon exerted to colloids is described by DLVO theory (after its authors **D**eryagin, **L**andau, **V**erwey and **O**verbeek). The DLVO theory takes into account the influence of electrostatic forces, Brownian motion and Van der Waals forces affecting the particles. The charged particles are surrounded by a coat of counter ions originating from the dispersion medium and thus forming electric double layer. The electric double layer is illustrated in Fig. 8. The first layer (adhering right to the surface of the particle) of counter ions is called Stern layer. The more distant (less rigidly adhering) counter ions form diffuse layer around the particle. The electrokinetic potential at the frontier between

diffuse layer and medium is called ζ - potential (Zeta - potential) and it is important characteristic in description of stability of lyophobic colloids [15].

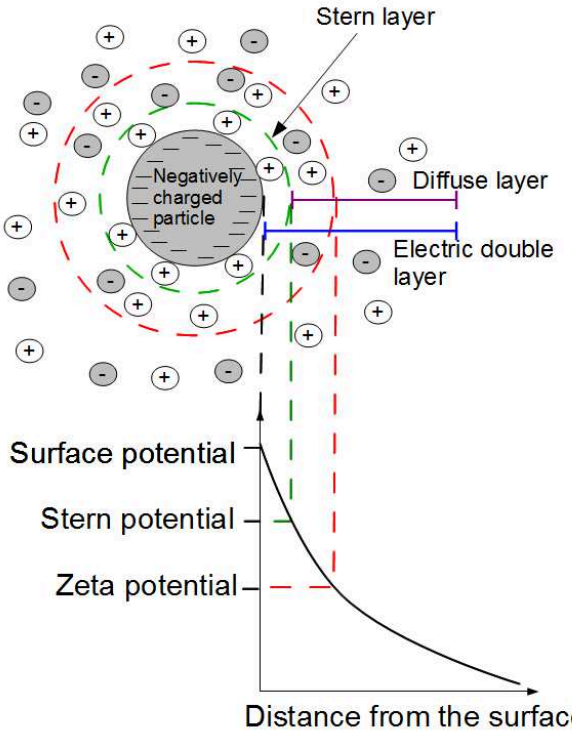

Fig. 8 The composition of electric double layer around particle.

Steric stabilization – is based on adsorption of suitable molecules on the whole surface of particles. These molecules are adsorbed on the particles but they are also soluble in the dispersion medium. Principle of this method is mechanical obstruction of closing particles near together shown in Fig. 9 where the attractive forces could prevail. The process of steric stabilization is often accomplished by adsorption macromolecules on the surface of the particle [15].

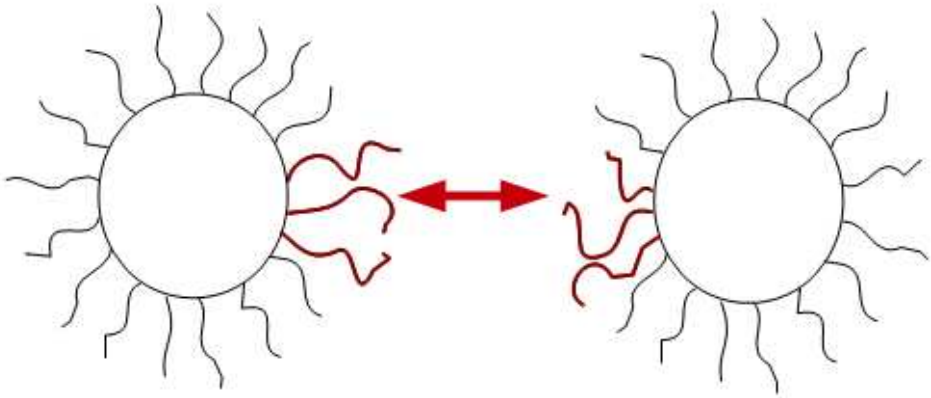

Fig. 9 Stabilization of particles through macromolecule adsorption (steric stabilization).

Factors affecting stability of the colloids- Electrostatic stability can be disrupted by addition of the electrolyte in the suitable medium and countering the repelling charges.

Electrostatic stability is very sensitive to the addition of electrolyte. The lowest concentration of added electrolyte that counteracts the charge and induces coagulation is called coagulation threshold. Steric stability is not very sensitive to electrolyte addition and temperature fluctuations and maintains its effect in different types of solvent (inorganic or organic unlike electrostatic stabilization). The down side of steric stabilization is contamination of the sample by stabilizing agent and difficulties with reversing the stabilization [15].

2.4 Titanyl sulphate

The precursor used for preparation of TiO_2 within the experimental part of diploma thesis is titanyl sulphate, also known as Titanium sulfate, basic; Titanium(IV)oxysulfate; Titanyl sulfate hydrate. The chemical formula of titanyl sulphate is $TiOSO_4.nH_2O$, its structure is schematically illustrated in Fig. 10. The CAS registry number is 13825-74-6. It is a white colored odorless fine powder. During the dilution of titanyl sulphate in water heat is released and solid $TiOSO_4.nH_2O$ may also precipitate. Titanyl sulphate in the liquid form contains sulfuric acid, whereas sufficient concentration of H_2SO_4 prevents precipitation of $TiOSO_4.nH_2O$ and its hydrolyzation. The titanyl sulphate solution is colorless liquid, corrosive to metals and tissue and causes severe skin burns and eye damage. Eye protection and protective clothing during the manipulation with this substance is necessary [2].

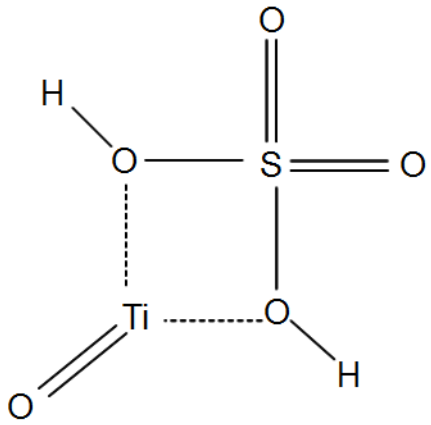

Fig. 10 Titanyl sulphate formula [17].

2.5 Preparation methods

Industrial production of pigment TiO_2 employs sulphate and chloride method [9]. As this thesis has been created in collaboration with industrial partner Precheza a.s. the emphasis is posed on the sulphate method that is utilized in this company for TiO_2 white pigment manufacturing.

Chloride method:

The first step in the method is the preparation of the titanium precursor. Raw material which is rich on titanium dioxide is converted to titanium tetrachloride ($TiCl_4$) in reduction atmosphere. Titanium dioxide reacts with chlorine according to chemical reaction (2). The reaction temperature has to be maintained at 800-1200 °C.

$$TiO_2 + 2\ Cl_2 + C \rightarrow TiCl_4 + CO_2 \quad (2)$$

The reaction gases are cooled and the separation of accompanying chlorides via sublimation or condensation at temperatures < 300 °C takes place. The $TiCl_4$ condenses at 0 °C and undergoes further purification.

Pigment grade TiO_2 is produced by the combustion of the separated $TiCl_4$ vapors in oxygen atmosphere at 900-1400 °C according to equation (3).

$$TiCl_4 + O_2 \rightarrow 2\ Cl_2 + TiO_2 \quad (3)$$

The prepared TiO_2 is caked on the sides of the reactor and is then subjected to further post treatment.

The determining factors affecting the particles size and its distribution during the chloride process are reaction temperature, oxygen excess and flow conditions in the reactor. Nuclei formation is affected by presence of water and Cs-compounds in $TiCl_4$ during combustion. Addition of aluminium chloride ($AlCl_3$) during the combustion promotes rutile formation on contrary to phosphorus trichloride (PCl_3) and silicon tetrachloride ($SiCl_4$) that are used to suppress formation of rutile in favor to anatase.

The chloride process produces TiO_2 pigments which have better lightness and more neutral hue than TiO_2 produced by sulphate process [9].

Sulphate method:

The sulphate process starts with preparation of the raw materials (ilmenite is used most often) which are dried to achieve the moisture content less than 0.1 % and grinded in a mill to particles of size around 40 μm. Prepared raw material is leached in the presence of concentrated sulfuric acid (80-98 % H_2SO_4) according to chemical reaction (4). The amount of the sulfuric acid is carefully measured in order to have the "acid number" (weight ratio of free H_2SO_4 to TiO_2 produced by the hydrolysis) in the range between 1.8-2.2. The hydration heat rises the temperature to 50-70 °C and the exothermic sulfate formation further increases the temperature to 170-220 °C [8, 18, 19].

$$FeTiO_3 + 2\ H_2SO_4 \rightarrow FeSO_4 + TiOSO_4 + 2\ H_2O \quad (4)$$

The reaction mixture is then left to mature for 1-12 hours depending on the starting raw material. The obtained cake is dissolved in cold water or diluted sulphur acid. The temperature is kept under 85 °C to prevent hydrolysis (especially with ilmenite as a starting raw material).

The iron presented in the trivalent form Fe^{3+} undergo hydrolyzation and adheres to titanium oxide hydrate, to prevent this phenomenon the Fe^{3+} is reduced to Fe^{2+} by scrap iron as shown in chemical reaction (5)[8, 18, 19].

$$Fe_2(SO_4)_3 + Fe^0 \rightarrow 3\ FeSO_4 \quad (5)$$

Reoxidation of Fe^{2+} is prevented by Ti^{3+}. The solution is left to settle and then filtered. All undissolved solid material is removed. Afterwards, the solution is cooled under vacuum and copperas ($FeSO_4.7H_2O$) crystallizes and is filtered see chemical reaction (6) [8, 18, 19].

$$FeSO_4 + 7\ H_2O \rightarrow FeSO_4 \cdot 7\ H_2O \quad (6)$$

The titanyl sulphate is hydrolyzed as described in reaction (7) at 94-110 °C and hydrated titanium dioxide (HTD) ($TiO(OH)_2$) is precipitated [8, 18, 19].

$$TiOSO_4 + 2\ H_2O \rightarrow TiO(OH)_2 + H_2SO_4 \quad (7)$$

Precipitated HTD has to be filtered and washed from impurities by water or diluted sulphur acid. The impurities that are not washed out can be removed by reduction in diluted sulphur acid at 50-90 °C with addition of zinc or aluminium powder or nonmetallic reducing agents. Chemisorbed sulphuric acid is removed during heating at high temperatures [9]. Some specific pigment grade may require additional treatment and dopation by alkali metals, phosphoric acid (H_3PO_4), zinc oxide (ZnO), aluminium oxide (Al_2O_3) or antimony trioxide (Sb_2O_3).

The water content in pure or doped hydrated titanium oxide is lowered by the treatment in rotary vacuum filters till it reaches approx. 30-40 % and then is calcined in rotary kiln at 800-1100 °C for several hours (7-20 h) [8, 18, 19]. The calcination of the product obtained after filtration proceeds according to reaction (8).

$$TiO(OH)_2 \rightarrow TiO_2 + H_2O \tag{8}$$

The determining factors affecting the rutile content, rutile particle size, in the sulphate process are hydrolysis progress (Eq. 7), purification of the hydrolysate, operating regime of the kiln and grinding of the product [8, 18, 19]. Entire process of TiO_2 production using sulphate method is schematically shown in Fig. 11.

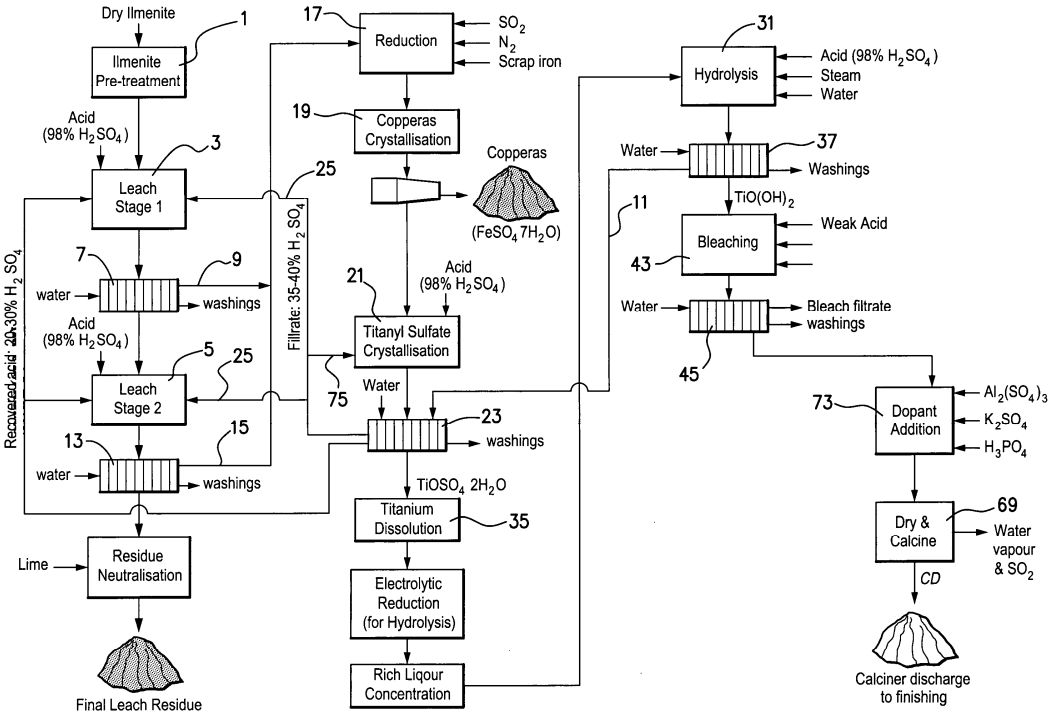

Fig. 11 Scheme of the sulphate method for TiO_2 production [18].

2.6 Precipitation

Hydrolysis is the most important reaction in the sulphate process of TiO_2 production and even though it is known for more than 80 years it has not been sufficiently described yet [20, 21]. Hydrated titanium dioxide (HTD) also known as metatitanic acid is formed during the hydrolysis of titanyl sulphate. The process follows chemical reaction (9). In the notation different from the one used in chemical reaction (7), the HTD can be written as $TiO.nH_2O$ and corresponding form of hydrolysis reaction is shown in reaction (9) [22].

$$TiOSO_4 + (n+1)\ H_2O \rightarrow TiO_2 \cdot n\ H_2O + H_2SO_4 \quad (9)$$

At the first stage "induction period", HTD is precipitated in colloid form. When the concentration of colloid HTD is sufficient, the growth of crystallite HTD starts "rapid hydrolysis", utilizing colloid particles as nucleation centers. The aggregation of HTD crystallites leads to the precipitation of TiO_2 from the solution [22]. The progress of the precipitation is illustrated by reaction (10).

$$TiOSO_4 \rightarrow TiO_2 \cdot n\ H_2O_{colloid} \rightarrow TiO_2 \cdot n\ H_2O_{crystallin\ e} \quad (10)$$

The growth mechanism of colloid particles has been addressed in chapter 2.3.3 "Particle growth".

Precipitation is affected by number of parameters, known parameters affecting the precipitation are:

- **Titanyl sulphate concentration** - increase in concentration of $TiOSO_4$ leads to decrease of hydrolysis degree (it has a negative effect on HTD formation) [23]. The $TiOSO_4$ concentration has great influence on the form of titanium ions in the solution. At high concentration of $TiOSO_4$ the titanium ions form long chains of –Ti^{2+}–O–Ti^{2+}–O–, at lower concentrations the titanium ions form monomers. The solubility of chains is lower than of the monomers [22].
- **Sulphuric acid concentration** - the sulfuric acid is required to prevent premature hydrolysis of the titanyl sulphate solution. It is characterized by "acid number" describing the ratio of sulfuric acid concentration (free and also bound in titanyl sulphate) to titanium dioxide and it is kept in range 1.8 - 2.2 [22].
- **Reaction temperature** - increased temperature improves the yield and shortens the time required for complete precipitation, at temperatures below 90 °C the precipitation is slowed down [22].
- **Crystallization seeds** - The presence of crystallization seeds, nucleation seeds, or centers is vital for the hydrolysis process. There are two methods of securing sufficient concentration of nucleation centers - the Mecklenburg method [20] and Blumenfeld method [21]. The Mecklenburg method is based on the preparation of the nucleation centers in the primary solution of titanyl sulphate. The Blumenfeld method is based on the preparation of the nucleation centers in the separate reactor and their subsequent transfer to the primary solution of titanyl sulphate [22].
- **Impurities** - the presence of Fe^{2+} during the hydrolysis has positive effect on formation of colloidal TiO_2 [22].

- **Stirring** - has no direct effect on the nucleation and size of the primary particles, but the stirring rate affects the size of agglomerates. With high stirring rate, the size of agglomerates decreases [22].

2.7 Characterization

The morphology, chemical composition and physical properties are always studied using different kinds of experimental methods. The basic principles of the employed characterization methods are described below.

2.7.1 X-ray diffraction

Standard method used for structure and phase analysis of powder sample is X-ray powder diffraction. This method utilizes photon diffraction on ordered atomic planes. The condition of organized structure is well met in crystalline solids but not in amorphous solids for their lack of long range organization. The method is not very suitable for them. Diffraction on crystal is expressed in Bragg equation (2)

$$n\lambda = 2\ d\ \sin\theta \tag{2}$$

where n is an integer, λ is wavelength of the incident light, d is spacing between planes and θ is an angle between incident beam and atomic plane.

The diffraction phenomenon can occur only if the photon has sufficient energy so that its wavelength according to equation (1) corresponds to the atomic size (1.10^{-10}m).

The source of X-ray photons is usually an X-ray tube where electrons are accelerated by a high voltage and collide with metal anode which leads to X-ray photons emission. Through the selection of anode and voltage regulation, it is possible to affect the energy of the photon. To prevent fluorescence the energy has to be carefully chosen. Diffracted rays are detected and the dependence of the signal intensity on scattering angle is registered. Brag-Brentano setup is very often used for phase analysis of powder samples and is schematically illustrated in Fig. 12.

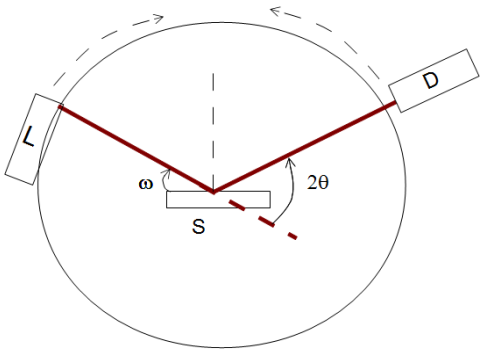

Fig. 12 Bragg-Brentano instrumental setup, where L is X-ray lamp, S sample, D detector, ω incident angle and 2θ scattering angle.

From diffraction patterns it is possible to determine crystallographic structure, crystallite size and by application of Rietveld method even parameters like texture and microstrain [24, 25].

2.7.2 Sulphur analysis

Sulphur content is often determined by combustion method. This method is based on heating of the weighted sample in oxygen stream, conversion of sulphur into sulphur dioxide SO_2 and infrared spectroscopic analysis of exhaust gases. Determined content of SO_2 is then recalculated to sulphur content. There are two possibilities for heating of the samples being analyzed i) heating in a resistance furnace or ii) heating in an induction furnace. In case of induction furnace, an accelerator is always added to the sample (e.g. tungsten or iron) so even non-conductive samples can be heated in the induction furnace.

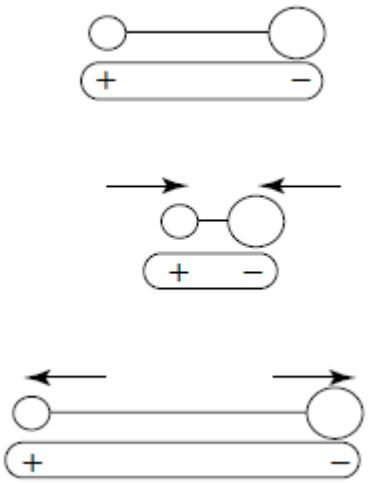

Fig. 13 Change in dipole moment of heteronuclear molecule [26].

During the analysis the released SO_2 molecules interact with infrared light (IR) in detector whereas the photon having the energies which match the transition energy of vibrational or

rotational modes induces dipole change in the molecule as is illustrated in Fig. 13. Each material has its characteristic IR spectrum with typical absorptions for bond lengths and symmetries [26]. Pros of this method is short measurement time and low consumption of sample, con of this method is the destruction of the sample and necessity for careful selection of proper calibration standards.

2.7.3 Measurement of the photodegradation activity

Photoactivity of the photocatalysts is evaluated based on the degradation of model pollutant under the irradiation. During photodegradation process the concentration of the model pollutant such as toluene, mono-nitrogen oxides (NO_x), organic dyes, etc. is decreased via the processes described in chapter 2.2 “Photoactivity”. The degradation process can take place in liquid medium (the photocatalyst is immersed or dispersed in pollutant solution) or in gas medium (solid photocatalyst placed in sealed reactor is exposed to stream of the gas pollutant) [14]. The photoactivity of one sample may differ for different pollutants and for gas and liquid medium. As was indicated in chapter 2.2 “Photoactivity”, the nature of the photodegradation process is rather complex and is affected by many factors. In this thesis, photoactivity was evaluated in liquid phase and organic dye was used as a model pollutant. The photodegradation effect was characterized using change in coloration of the photocatalyst and model dye aquatic suspension subjected to UV light irradiation.

Generally every possible color can be expressed as a combination of three basic colors (red, green, blue), their combination is called tristimulus and is described by parameters X, Y, Z, respectively. The ideal color space can be viewed as 3D object where every position corresponds to a color and is described by three co-ordinates. Several color spaces were devised and the most notable one is CIELAB recommended by Commission Internationale de l’Eclairage (CIE international authority on light and lighting, color and vision, photobiology and image technology). The CIELAB system can be described as 3D set of points, where every point represents a color and points are arranged in a way that distance between two points corresponds to the difference in their color (see Fig. 14).

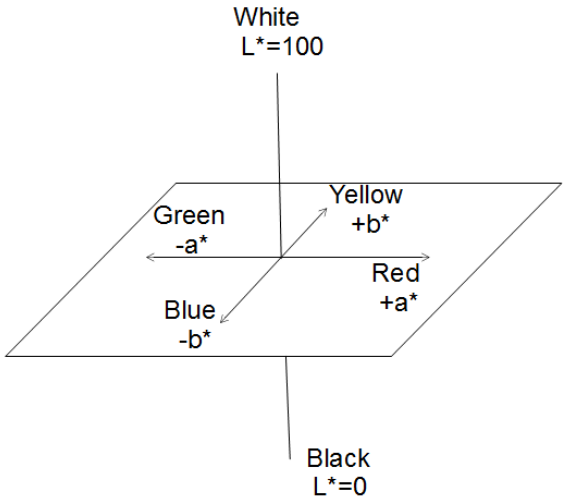

Fig. 14 CIELAB color space.

Every point in CIELAB space is characterized by parameters: L* lightness, a* position between red and green, b* position between blue and yellow. In ideal situation the discoloration of the dispersion is complete and the measured L*a*b* parameters of a suspension after the photodegradation experiment are identical with the values measured before addition of dye into the suspension. Unfortunately this state is not usually achieved because the presence of the dye fragments created during the photoinduced decomposition of dye. The dye fragments can be adsorbed on the surface of the catalyst and change its color or can block further adsorption of other chemical species [27, 28].

2.7.4 Thermal analysis

Thermal analysis (TA) methods are based on heating of the sample according to predetermined temperature program. The methods belonging to this group can be divided based on the monitored parameters during the sample heating into three basic categories:

a) methods measuring weight changes

b) methods determining the change in thermal properties

c) methods assessing changes of other parameters

Thermogravimetry (TG) belongs to method classified in a) section. The sample is placed in a crucible and is gradually heated with known temperature program. The changes in weight are carefully monitored and plotted as a function of temperature: $\Delta m = f(T)$. From the acquired data it is possible to determine the temperature at which the given weight change occurs and with the knowledge of elemental composition of the sample it is possible to identify what chemical reaction may have caused this weight change. The main factors

affecting TG thermogram are starting weight of the sample, temperature program, the sample geometry and furnace atmosphere.

Differential scanning calorimetry (DSC) belongs to method classified in b) section. This method is based on the measurement of electric input required for heating of the sample. Together with sample the selected standard material is placed in furnace both of them have separate heating source. The difference in power input between heating stage of sample and standard is measured. In case of endothermic reaction the sample absorbs more heat than standard and thus the power input into its heating stage has to be increased to compensate the difference between the heating stage of standard while in the case of exothermic reaction of sample it is the standard that needs increase of power input to minimize the temperature difference.

Thermal analysis methods are very useful for observing phase transitions, crystallization, determining hydratation, decomposition reactions, stability evaluation, determination of purity etc. On the other hand the thermogravimetry is time consuming method (samples have to be usually dried for at least 24 h and the main analysis also requires several hours) [29, 30].

2.7.5 Electron microscopy techniques

The principle of electron microscopy is similar to optical microscopy, but photons are substituted by electrons and focusation of the electron beam is done by electromagnetic coils. The electrons are thermally emitted from a tip of a metal filament and accelerated by high voltage towards the sample. The electromagnetic coils divert the electron beam over the sample surface. The electron beam interacts with electron shells of sample atoms. The whole variety of interactions that can take place during the interaction of emitted electron and surface of the sample is shown in Fig. 15.

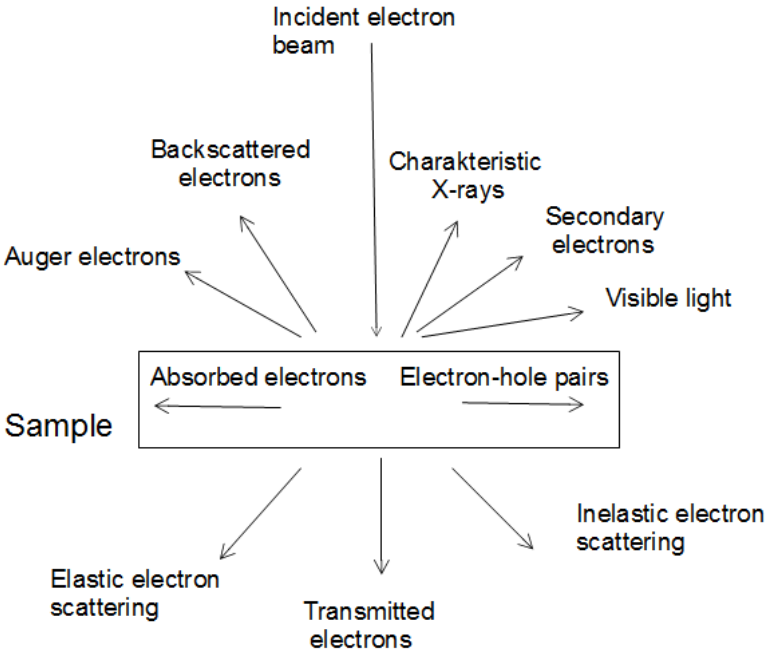

Fig. 15 The electron interaction with the sample.

Scanning electron microscopy (SEM) utilizes acceleration voltage commonly in the order of tenths of keV (typically 10-30 keV) whereas transmission electron microscopy (TEM) requires higher acceleration voltage about 80-400 keV. The SEM technique is used for determining of the morphology of the sample. The SEM microscope is usually equipped with EDX analyzer which enables determination of chemical composition. There are two major imaging modes used in SEM technique. The display in secondary electrons (SE) utilizes electrons knocked out from the electron shells in the sample. These electrons are due to their low energy prone to recombination and therefore give information from only thin surface layer of the sample. Imaging in back scattered electrons (BSE) which are electrons bounced back from the electron shell is preferred mode for observation of heavy elements. Chemical analysis can be determined from analysis of characteristic X- rays that are created when the electron from the beam knocks out one of the core shell electrons and the vacancy is filled by an electron from valence layer. The energy difference between those two electron states is emitted in the form of photon. The electron transitions in electron shell are characteristic for each chemical element. The method is called energy-dispersive X-ray spectroscopy (EDX) [31].

2.7.6 Specific surface area and porosity

As was shown in chapter 2.2 “Photoactivity” in Fig. 5 the adsorption and desorption on the semiconductor particle plays a vital role in the process of heterogeneous photocatalysis and one of the factors involved is specific surface area (SSA) defined as total surface area per

unit of mass. The specific surface area consists of external surface area of the particles and internal surface area of the pores. For most of porous materials the external surface area is usually much larger than the internal one but in microporous materials the situation is opposite [32].

The SSA of solids is commonly determined by gas physisorption (adsorbate - nitrogen or argon) on powder sample (adsorbent). The measured value of surface is influenced by used type of adsorbate, temperature and pressure. The physisorption is based on van der Waals interactions that have longer range than strong chemical bonds and allows formation of multilayers. According to different interactions between adsorbent and adsorbate the individual types of model adsorption isotherms were classified (IUPAC classification, see Fig. 16). Adsorption isotherms are functions of volume of adsorbate on gas pressure at constant temperature [32].

In Fig. 16 where I is isotherm describing adsorption on microporous adsorbent, II is isotherm describing adsorption on macroporous adsorbent with strong adsorbate - adsorbent interaction, III is isotherm describing adsorption on macroporous adsorbent with weak adsorbate - adsorbent interaction, IV is isotherm describing monolayer adsorption, multilayer adsorption and capillary condensation in mesoporous adsorbent with strong adsorbate - adsorbent interaction, V is isotherm describing monolayer adsorption, multilayer adsorption and capillary condensation in mesoporous adsorbent with weak adsorbate - adsorbent interaction, VI describes adsorption isotherm with several steps [33].

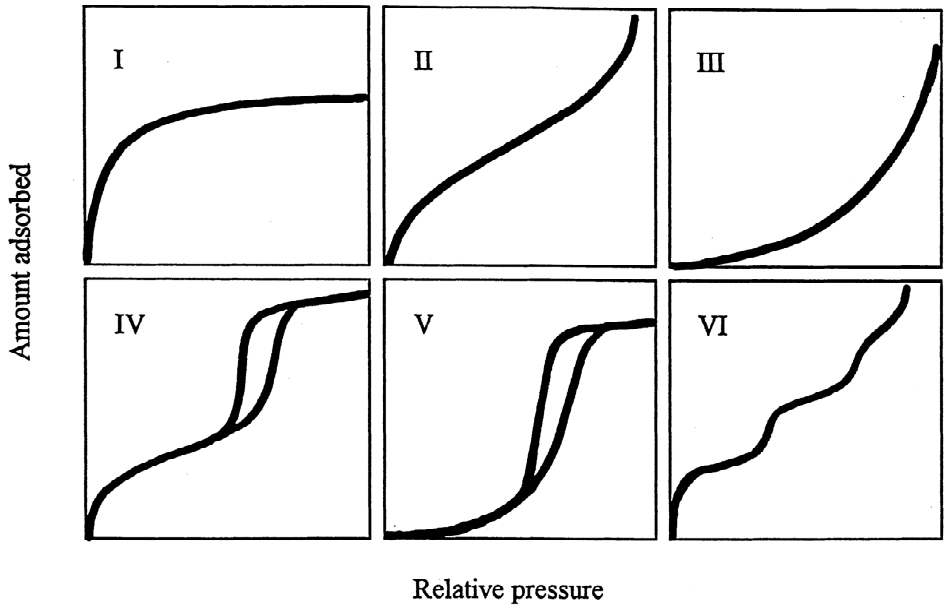

Fig. 16 Illustration of different isotherm functions [34].

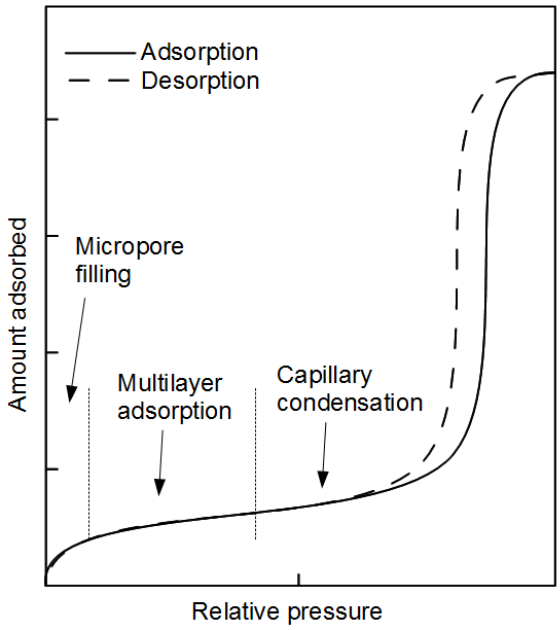

Fig. 17 The physisorption progress illustrated on IV isotherm [32].

Pore size and shape can be determined from the shape of isotherm and its hysteresis loop as is illustrated in Fig. 17. The volume of adsorbate adsorbed at maximum pressure is called net pore volume. According to diameter the pores are divided to macropores (pore diameter > 50 nm), mesopores (pore diameter from 2 nm to 50 nm) and micropores (pore diameter < 2 nm). Among well-accepted models of pore shapes belong the cylinder, the slit or ink-bottled [32].

The positive aspects of physisorption (SSA measurement by gas adsorption) are the ability to measure micropores in a nondestructive manner. The negative aspect is long time of measurement (i.e. 6 hours and more). Moreover, the samples before physisorption analysis have to be pre-treated, i.e. degassed at low vacuum and dried for several hours [32].

3 Experimental

The aim of the experimental work was preparation and characterization of photoactive TiO_2 from powder titanyl sulphate precursor using three synthesis methods. The synthesis processes, their variations as well as the results obtained using selected methods of chemical and phase analysis applied on precursor and products are described in this section. The synthesis methods were evaluated by the means of the photodegradation activity of resulting TiO_2.

The experimental methods of the $TiOSO_4$ characterization were chosen in order to determine the purity and the composition of this precursor material and to confirm the presence of TiO_2 in the products. The presence of impurities in TiO_2 products was analyzed and crystal structure, crystallite size, morphology, specific surface area and photoactivity was determined. The effect of thermal treatment on the structure and photocatalytic activity of prepared samples was also studied.

3.1 The characterization of precursor

Powdered titanyl sulphate obtained from Precheza a.s. was used as TiO_2 precursor in all three synthesis methods. This precursor was prepared using the sulphate process and was of very high quality. The phase composition and the presence of impurities was evaluated using XRD and TG/DSC-MS analysis.

3.1.1 X-ray diffraction

The phase composition of the powder $TiOSO_4$ was determined using X-ray powder diffraction. The XRD pattern was obtained using Bruker D8 Advance diffractometer (Bruker AXS, Germany) with fast position sensitive detector VÅNTEC 1, photo of the instrument is shown in Fig. 18.

The source of X-ray irradiation was cobalt tube (CoKα, $\lambda = 1.7889$ m^{-10}). The powder titanyl sulphate sample was pressed in rotational holder and measured in the reflection mode. The registered XRD pattern was evaluated using the database PDF 2 Release 2012 (International Centre for Diffraction Data).

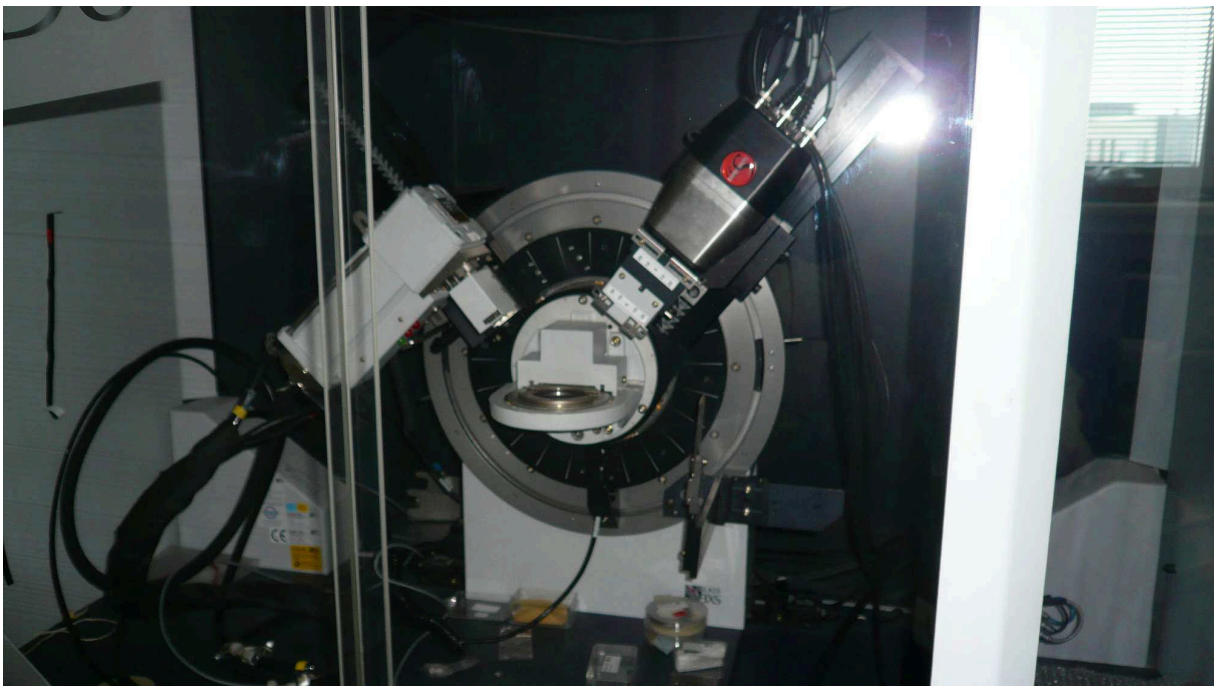

Fig. 18 Photo of Bruker D8 Advance X-ray diffractometer.

The registered XRD pattern of $TiOSO_4$ precursor is shown in Fig. 19. All of the registered diffraction lines correspond with the entry for titanyl sulphate monohydrate (card no. card 81-1567) in the PDF 2 database, card 81-1567 is included in attachments.

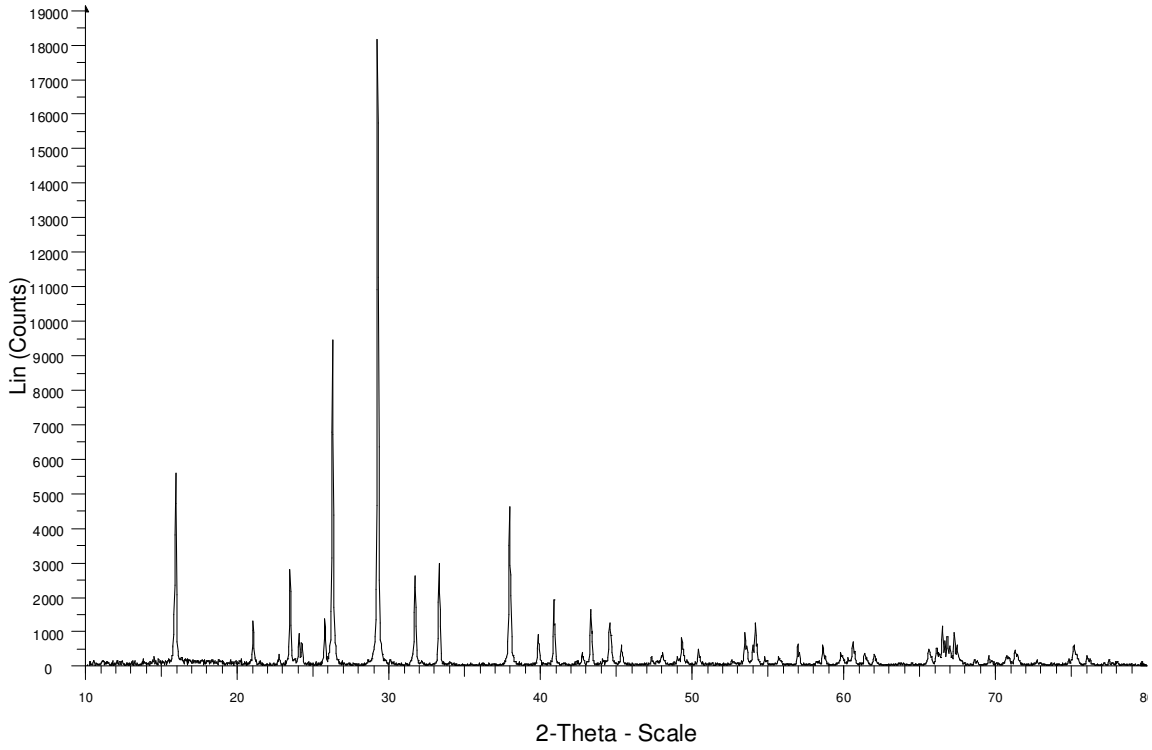

Fig. 19 XRD pattern of titanyl sulphate monohydrate.

3.1.2 Thermal analysis

Thermogravimetric analysis (TG) and differential scanning calorimetry (DSC) of $TiOSO_4$ were measured using instrument Netzsch-Gerätebau GmbH - STA 449 C Jupiter Thermo-microbalance equiped with mass spectrometer detector. The sample (10.560 mg) was placed into the α-Al_2O_3 sample holder and was heated in dynamic atmosphere of the mixture of nitrogen and oxygen (flow of oxygen - 50 mL/min, flow of nitrogen - 15 mL/min of nitrogen). The heating rate was 10 °C/min. The maximum temperature was set to 1200 °C. The registered TG-DSC-MS curves are shown in Fig. 20.

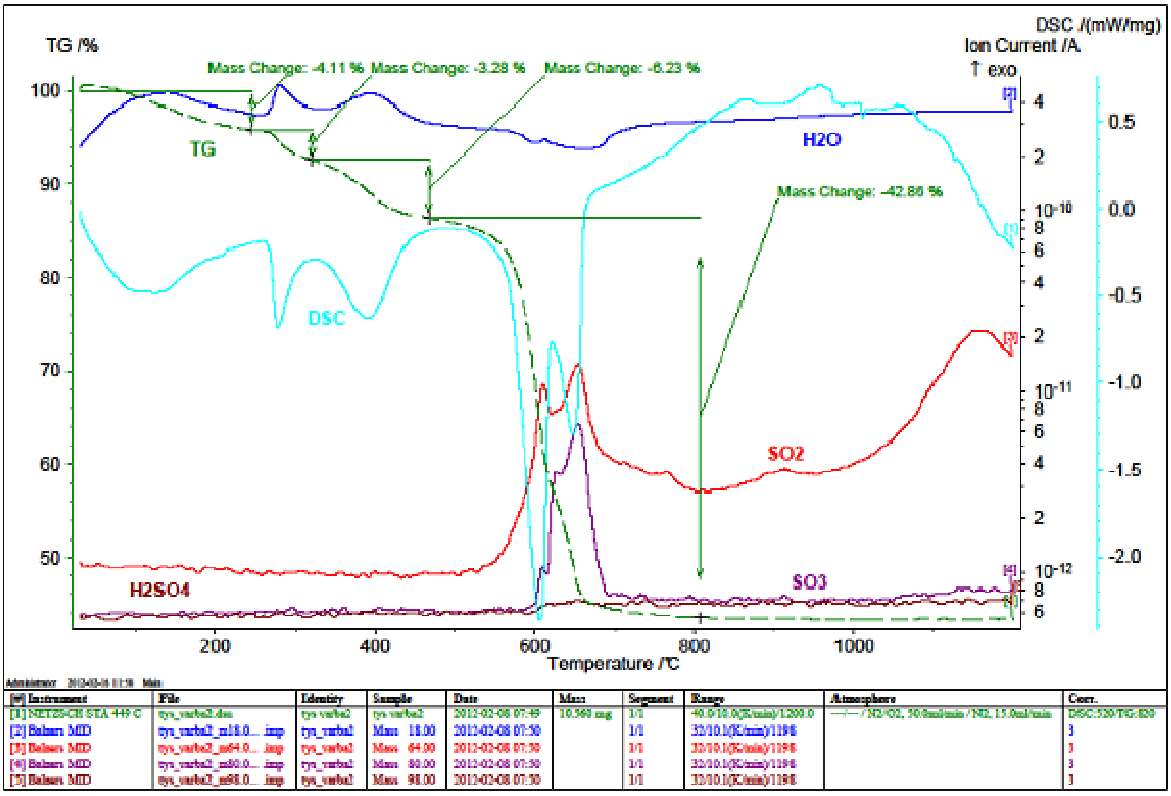

Fig. 20 Thermogravimetric analysis of titanyl sulphate.

TG curve (Fig. 20) reveals four distinct drops of weight in whole temperature range. The weight losses at 250 °C, 325 °C and 475 °C are attributed to release of water as revealed by MS spectra (Fig. 20). The overall decrease of weight up to 475 °C, attributed to the release of water, is 13.6 wt%. In pure titanyl sulphate monohydrate the amount of water should be 10.1 wt%. With respect to the XRD the titanyl sulphate should be monohydrate, but the loss of water 13.6 wt% theoretically corresponds to hydrated titanyl sulphate of formula $TiOSO_4 \cdot 1.4H_2O$. The discovered difference can be explained by the presence of physically adsorbed water in total amount 3.5 wt% what also correlates with acidic character of titanyl sulphate. The presence of the titanyl sulphate with higher amount of crystalline water (e.g.

$TiOSO_4 \cdot 5H_2O$) in the $TiOSO_4$ precursor in the amount which is undetectable with XRD method can be another reason for higher amount of water detected by TG analysis. The sulphur in the form of sulphur oxides is released at temperatures above 600 °C as evident from TG and MS curves (Fig. 20). The DSC curve shows endothermic desorption of water and exothermic decomposition of the titanyl sulphate accompanied with release of sulphur oxides [29].

3.2 Synthesis methods

Three synthesis methods used for preparation of TiO_2 in the experimental part are based on method published by Sivakumar et al. [35]. The original method used by Sivakumar et al. was modified in the neutralization step where ammonium hydroxide (NH_4OH) was replaced by sodium hydroxide (NaOH). With the idea of possible industrial production in the future, the sodium hydroxide presents more ecological alternative to dangerous ammonium hydroxide.

The powder titanyl sulphate precursor was diluted to liquid titanyl sulphate. The preparation of liquid titanyl sulphate comprises dissolution of powder titanyl sulphate supplied by Precheza a.s, in weak acid solution (0.5 wt% H_2SO_4) to give the final concentration (0.2 $mol \cdot dm^{-3}$ TiO_2) where the presence of sulphuric acid prevented hydrolyzation. The aqueous suspension of $TiOSO_4$ was agitated overnight (22 h).

The first synthesis is directly based on the Sivakumar´s et al. [35] method which was modified in the neutralization step where ammonium hydroxide (NH_4OH) was replaced by sodium hydroxide (NaOH). The synthesis is designated as synthesis No.1 and in detail is described in chapter 3.2.1.

The second synthesis utilized information discussed in chapter 2.6 “Precipitation” and the reaction temperature was raised. The reaction temperature was elevated in order to accelerate hydrolysis in the precipitation step. The temperature 80 °C proved to be sufficient to start spontaneous hydrolysis. The synthesis is designated as synthesis No.2. and in detail described in chapter 3.2.2.

The third synthesis employed also reaction at elevated temperature combined with the effect of nucleation seeds. The Mecklenburg method of nucleation seeds preparation in a primary solution was applied. The synthesis is designated as synthesis No.3 and in detail is described in chapter 3.2.1.

The final products of all of the synthesis were rinsed with water to wash out sulphate ions (SO_4^{2-}) present from the sulphuric acid. The presence of sulphate ions was tested using

barium chloride ($BaCl_2$) solution, where Ba^{2+} ions react with SO_4^{2-} ions to give white precipitates of $BaSO_4$ which is almost insoluble in water.

Rinsed products were dried at 105 °C for 1 h and thermally treated at selected temperatures. The samples were calcined in muffle furnace at temperatures 200, 400, 600 and 800 °C for 1 h. Heat treated samples were distinguished with suffixes to their title stating maximum temperature during the heat treatment. The suffix used for samples dried at 105 °C was 105, for samples calcined at 200, 400, 600 and 800 °C suffixes K200, K400, K600 and K800 respectively were used.

The dried and calcined samples (4 g of dried sample or 1 g of calcined sample) were individually put into boron nitride grinding bowl with 5 balls and milled for 15 minutes in planetary mill Pulverisette 7 from Fritsch .

3.2.1 Synthesis No.1

The synthesis No.1 is schematically shown in Fig. 21. The 2 L of 0.2 mol·dm^{-3} solution of titanyl sulphate was neutralized with 20 wt% solution of NaOH to reach the pH value of 7 at constant rate of agitating using overhead stirrer (300 rpm). It has to be mentioned that during the neutralization the solution was overtitrated by NaOH and pH = 7 had to be restored by the addition of conc. sulphuric acid. During the neutralization process the precipitation of $TiO(OH)_2$ occurred. The resulting precipitate was filtrated and the filter cake was rinsed with demineralized (demi) water with the aim to remove sulphate ions. The presence of sulphate ions in filtrate was tested using aqueous solution of barium chloride ($BaCl_2$) with concentration 10 wt% of $BaCl_2$. The sample was rinsed with 7 L of demi water before the sulphate test was negative. The cake was afterwards subjected to drying, calcination and milling. According to heat treatment the produced samples were denoted as TiO_2 K105, TiO_2 K200, TiO_2 K400, TiO_2 K600 and TiO_2 K800.

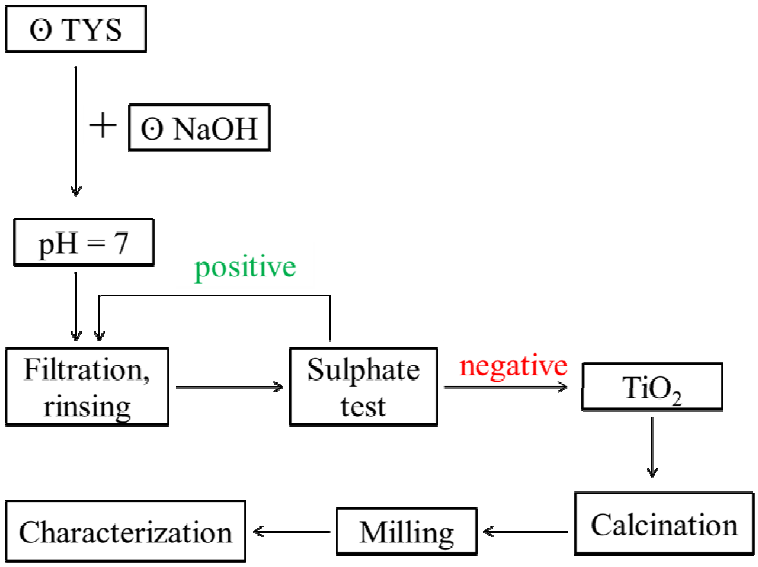

Fig. 21 Scheme illustrating synthesis No. 1.

3.2.2 Synthesis No.2

The synthesis No.2 is schematically shown in Fig. 22 and represents modification of synthesis No.1. The modification is based on raising the temperature of the titanyl sulphate when 2 L of 0.2 mol·dm^{-3} solution of titanyl sulphate was heated up to 80 °C at constant stirring (300 rpm). The spontaneous precipitation of $TiO(OH)_2$ occurred. The precipitation was supported by neutralization using aqueous solution of NaOH (20 wt%) to reach the pH 7. The precipitate was filtrated, and filter cake was rinsed with demi water. The presence of sulphate ions in filtrate was tested by 10 wt% barium chloride ($BaCl_2$) solution. The sample was rinsed with 7 L of demi water before the sulphate test was negative. The cake was afterwards subjected to drying, calcination and milling. According to heat treatment the produced samples were named TiO_2-T 105, TiO_2-T K200, TiO_2-T K400, TiO_2-T K600 and TiO_2-T K800.

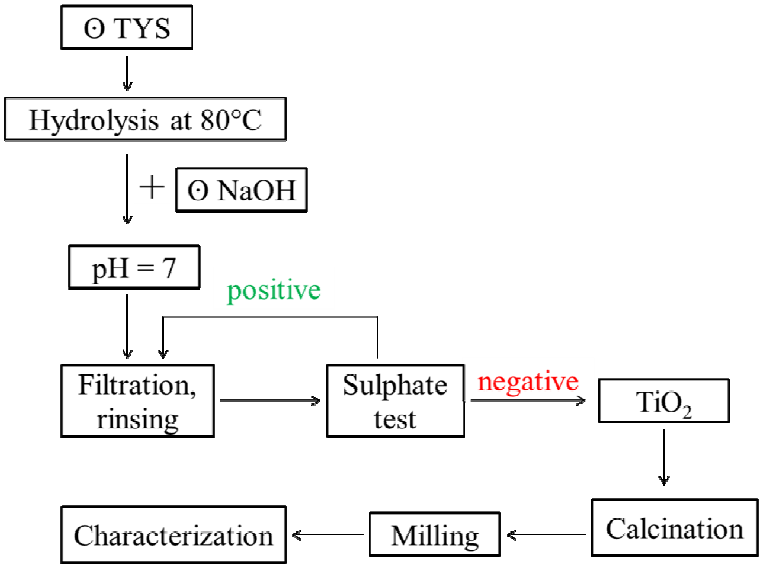

Fig. 22 Scheme illustrating synthesis No.2.

3.2.3 Synthesis No.3

The synthesis No.3 is schematically shown in Fig. 23. In this synthesis 2L of 0.2 mol·dm^{-3} solution of titanyl sulphate was dropwise added into 800 mL of 10 wt% NaOH aqueous solution by peristaltic pump in the time interval of 80 min. In the course of this mixing the mixture was stirred at a constant rate of 300 rpm using overhead stirrer. This led to creation of nucleation centers in the reaction mixture. After the mixing was completed, the reaction mixture was heated to the boiling point and then left to cool to 80 °C to further advance $TiO(OH)_2$ precipitation on the nucleation centers. The pH of the suspension was adjusted by addition of 13 mL of conc. sulphuric acid to give the pH 7. The resulting precipitate was filtrated and filter cake was rinsed with demi water. The presence of sulphate ions in filtrate was tested by 10 wt% barium chloride ($BaCl_2$) solution. The sample was washed with 10 L of water before the sulphate test was negative. The cake was afterwards subjected to drying, calcination and milling. According to heat treatment the produced samples were named TiO_2-MZ 105, TiO_2-MZ K200, TiO_2-MZ K400, TiO_2-MZ K600 and TiO_2-MZ K800.

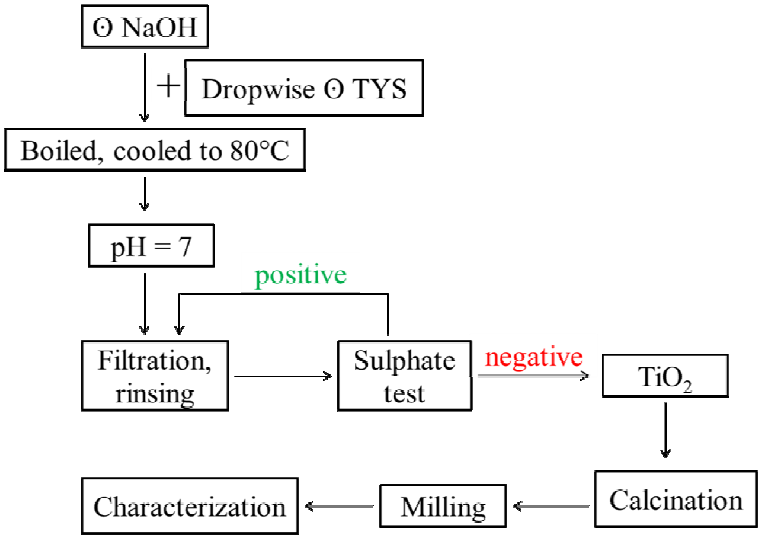

Fig. 23 Scheme illustrating synthesis No.3.

3.3 The characterization of the products

Morphology, chemical composition and physical properties of the TiO_2 produced by syntheses No.1 – No.3 were characterized and evaluated using X-ray diffraction, sulphur analysis, photodegradation activity measurement, thermal analysis, scanning electron microscopy and physisorption.

3.3.1 X-ray powder diffraction

The XRD patterns were plotted from data measured using the same instrumental apparatus as was used for characterization of the precursor (see chapter 3.1.1.). The XRD patterns of the samples prepared using synthesis No. 1, No. 2 and No. 3 and samples obtained after their calcination are shown in Fig.24, Fig. 25 and Fig. 26, respectively. The amorphous character of the dried samples (TiO_2 105, TiO_2-T 105, TiO_2-MZ 105) is clearly evident from their diffraction patterns, whereas the lowest crystallinity (highest amorphous character) shows the sample TiO_2-MZ 105. Although the samples show amorphous character the diffraction lines belonging to anatase can be observed on the diffraction patterns of the samples TiO_2 105 and TiO_2-T 105.

The samples prepared using syntheses No.1 and No.2 consists only of anatase up to 600 °C, whereas complete phase transformation of anatase to rutile was observed after the calcination at 800 °C for both syntheses methods, also the samples calcined at 800 °C consists of newly originated sodium hexa-titanate ($Na_2Ti_6O_{13}$). The sample prepared by method No. 3 does not show the rutile formation even at 800 °C but shows the formation of sodium hexa-titanate ($Na_2Ti_6O_{13}$) already at 400 °C.

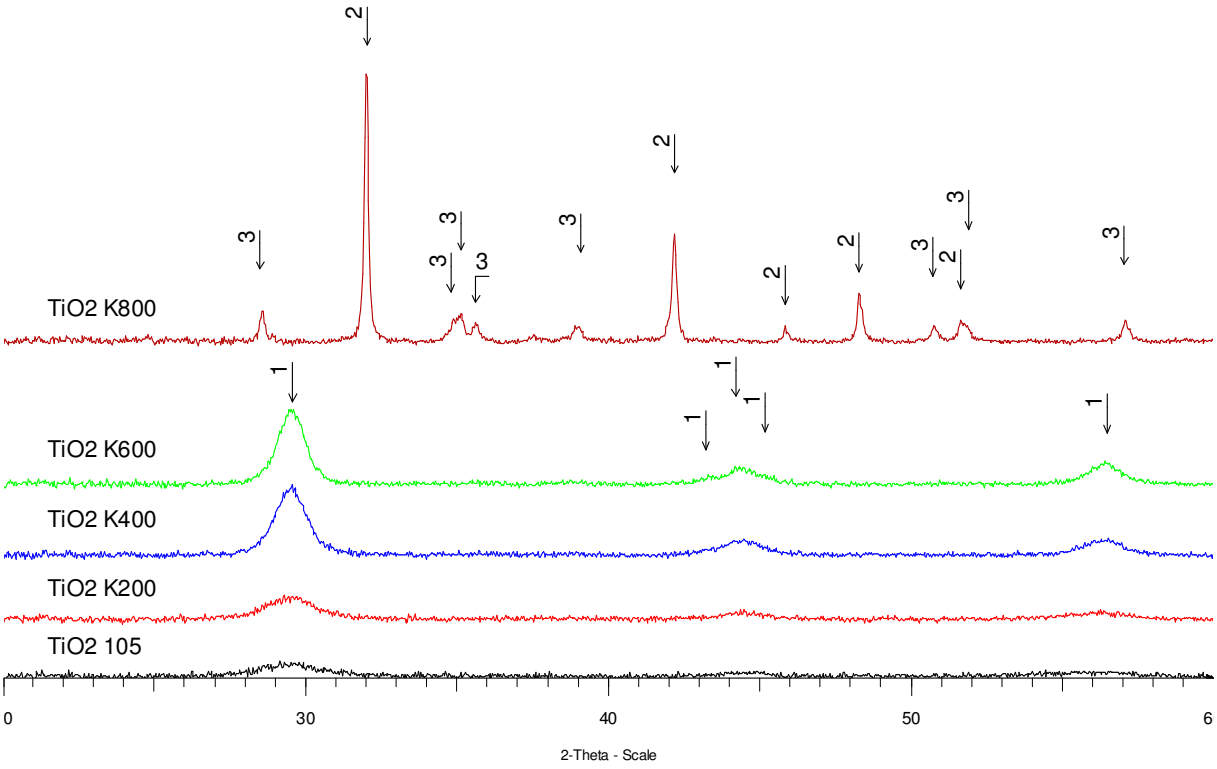

Fig.24 XRD patterns of TiO_2 powder samples prepared by synthesis No.1 where 1 is anatase, 2 is rutile, and 3 is sodium hexa-titanate.

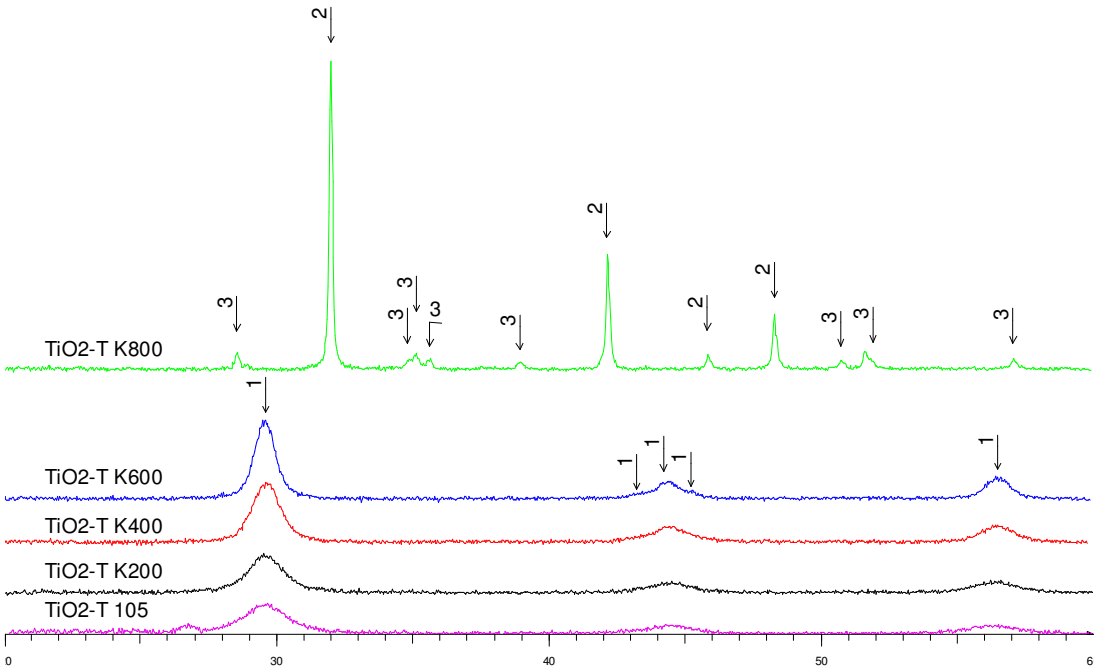

Fig.25 XRD patterns of TiO_2 powder samples prepared by synthesis No.2 where 1 is anatase, 2 is rutile, and 3 is sodium hexa-titanate.

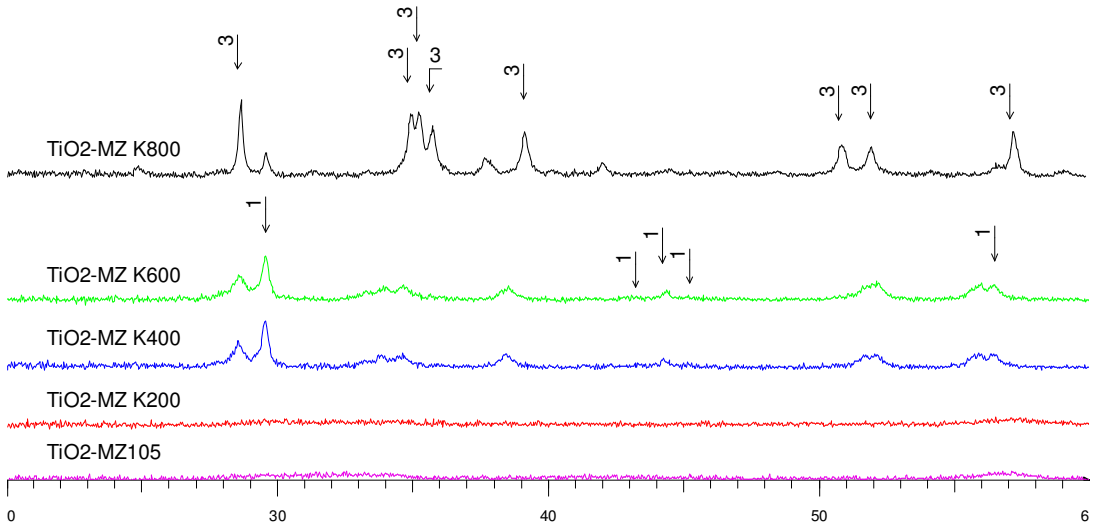

Fig. 26 XRD patterns of TiO_2 powder samples prepared by synthesis No.3 where 1 is anatase, and 3 is sodium hexa-titanate.

Heat treatment of the samples prepared using all of the three methods increased crystallinity (crystallite size) of the TiO_2. Average size of anatase crystallites (L_c) was calculated using equation (3) proposed by Scherrer [36].

$$L_C = \frac{K \times \lambda}{FWHM \times \cos\theta} \tag{3}$$

Where K is shape factor (for spherical particles is $K = 0.89$), λ is the X-ray wave length (in case of CoKα irradiation: $\lambda = 0.17889$ nm), θ is Bragg angle in radians, *FWHM* stands for full width at half maximum of the (101) anatase diffraction peak. The anatase crystallite size (L_c) calculated for the prepared powder samples is shown in Tab. 2.

Tab. 2 The anatase crystallite size L_c (nm)

Synthesis No.1	L_c	Synthesis No.2	L_c	Synthesis No.3	L_c
TiO_2 105	6.3	TiO_2-T 105	6.0	TiO_2-MZ 105	---
TiO_2 K200	8.9	TiO_2-T K200	7.2	TiO_2-MZ K200	---
TiO_2 K400	11.1	TiO_2-T K400	8.8	TiO_2-MZ K400	62.1
TiO_2 K600	9.9	TiO_2-T K600	11.8	TiO_2-MZ K600	59.4
TiO_2 K800	---	TiO_2-T K800	---	TiO_2-MZ K800	108.5

From the comparison of the calculated anatase crystallite size values in Tab. 2 the positive effect of heat treatment on crystallite size growing is apparent. The crystallite size of anatase increases with increasing temperature of the calcinations. The synthesis No.3 provides crystallites more than six times larger than other two methods.

It is well known that the presence of anatase and its crystallite size have significant influence on photocatalytic activity of TiO_2 [4]. With respect to crystallite size and growing content of anatase phase the sample TiO_2-T K400 should exhibit the best photocatalytic activity.

3.3.2 Thermal analysis

The thermal analysis of the dried samples TiO_2 105, TiO_2-T 105, TiO_2-MZ 105 was performed using the same instrumental apparatus as was used for characterization of the titanyl sulphate precursor (see chapter 3.1.2) and TG/DSC curves of these samples are compared in Fig. 27. It can be seen that the samples dried at 105 °C for 1 h contain significant amount of adsorbed water. The water is completely desorbed from the samples when the temperature exceeds 300 °C. The water content varies between samples. The largest content of adsorbed water (15 wt%) is presented in sample TiO_2-MZ 105 (TG curve is marked by violet color), the second largest water content (13 wt%) had the sample TiO_2 105 (TG curve is

marked by red color) and the lowest water content (12 wt%) had the sample TiO_2-T 105 (TG curve is marked by green color).

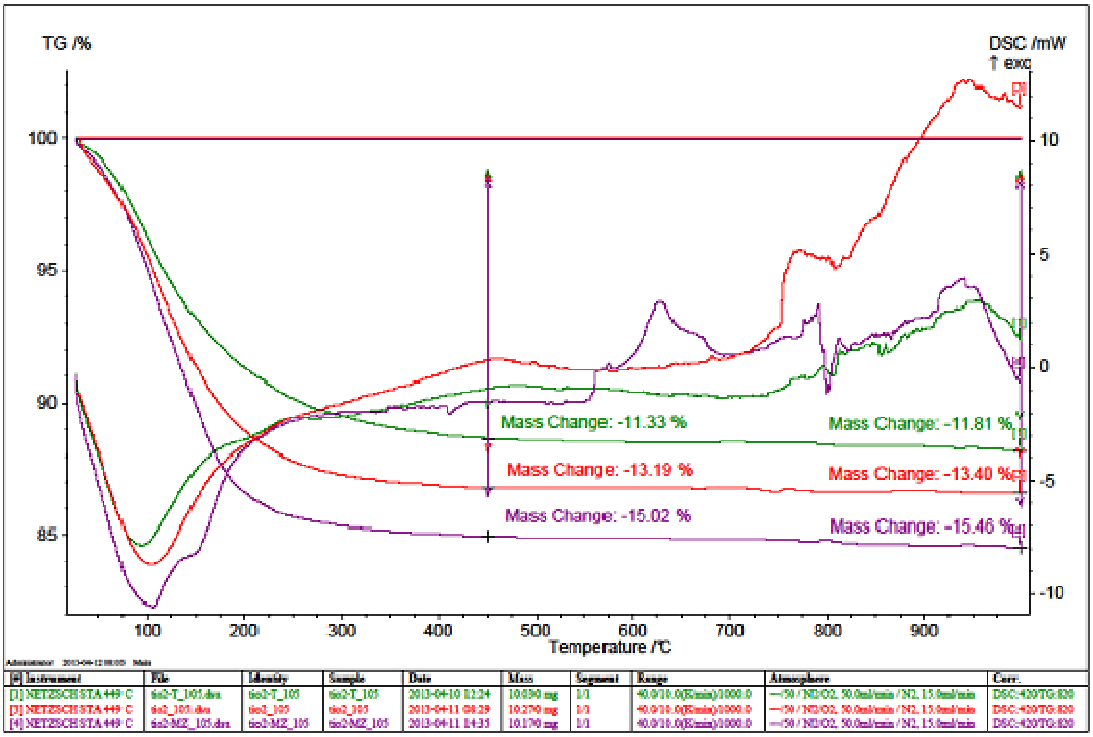

Fig. 27 Thermogram and DSC scan of dried samples TiO_2 105 (red line), TiO_2-T 105 (green line) and TiO_2-MZ 105 (violet line).

3.3.3 Sulphur analysis

The sulphur content was analyzed using Carbon Sulfur determinator ELTRA CS2000 supplemented with an induction furnace (Fig. 28). The combustion process was carried out in ceramic crucibles filled with 1 g of iron chip accelerator and 0.1 g of the sample.

Fig. 28 Photo of Carbon Sulfur determinator ELTRA CS2000.

The determined sulphur content is shown in Tab. 3. The sulphur content does not exceed 0.364 wt% and any trends in sulphur content and heat treatment temperature are not apparent. It can be concluded that most of the sulphur was washed out during the rinsing of filter cake with demi water.

Tab. 3 Sulphur content in wt%.

Synthesis no.1	Sulphur content	Synthesis no.2	Sulphur content	Synthesis no.3	Sulphur content
TiO_2 105	0.256	TiO_2-T 105	0.292	TiO_2-MZ 105	0.331
TiO_2 K200	0.316	TiO_2-T K200	0.339	TiO_2-MZ K200	0.249
TiO_2 K400	0.336	TiO_2-T K400	0.364	TiO_2-MZ K400	0.283
TiO_2 K600	0.232	TiO_2-T K600	0.299	TiO_2-MZ K600	0.258
TiO_2 K800	0.297	TiO_2-T K800	0.287	TiO_2-MZ K800	0.237

3.3.4 The measurement of the photodegradation activity

The photocatalytic activity of the prepared samples was measured according to Precheza a.s. internal protocol used for powder samples photoactivity measurement in water suspension in cuvette with 10 mm lightpath using UV-VIS spectrometer UltraScan XE-Hunter Lab in diffuse reflectance setup. This method is based on registration of the diffuse-reflectance spectra of the aqueous suspension of tested sample colored with acid orange 7 after the UV irradiation.

The testing suspension was prepared from 100 mL of demi water and 0.1 g of the powder sample, then 50 mL of this suspension was pipetted into beaker and stirred at 300 rpm for 5 min with electromagnetic stirrer, then the diffuse reflectance spectra of the suspension was measured and set as a baseline. Subsequently the suspension was colored by addition of 0.5 mL of model dye (c = 0.0015 mol/L acid orange 7). The obtained colored suspension was further stirred for 15 min before the photodegradation activity measurement begin. After this step the irradiation of the stirred suspension using UVA mercury lamp OSRAM L36-73 is initiated and the diffuse reflectance spectra are measured at first in 2 min. intervals to capture the beginning of the photodegradation process and 5 min. intervals after the stabilization. The measurement continued until the photodegradation of the dye was complete or until 120 minutes of exposition time passed. The photodegradation activity was evaluated from L*a*b coordinates in a form of time necessary for photodegradation. The table Tab. 4 shows the time calculated from the monitoring of the b* parameter in CIELAB color space. The value of b* parameter rose after the addition of dye to the suspension, subsequent decrease of the value in response to photodegradation of the dye was monitored.

Tab. 4 The photodegradation activity of the sample is described as a time necessary for photodegradation (min).

Synthesis no.1	Time	Synthesis no.2	Time	Synthesis no.3	Time
TiO_2 105	---	TiO_2-T 105	32.6	TiO_2-MZ 105	---
TiO_2 K200	---	TiO_2-T K200	26.2	TiO_2-MZ K200	33.1
TiO_2 K400	35.1	TiO_2-T K400	19.2	TiO_2-MZ K400	19.7
TiO_2 K600	46.0	TiO_2-T K600	20.6	TiO_2-MZ K600	26.9
TiO_2 K800	44.9	TiO_2-T K800	---	TiO_2-MZ K800	---

From Tab. 4 is clear that the most photoactive are the samples calcined at 400 °C. It has to be noted, that not for all of the samples was photodegradation activity successfully evaluated due to the sedimentation of the measured sample or adsorption of the dye and products of photodegradation at the surface of the samples what led to significant difference of diffuse reflectance spectra which were non-comparable with baseline spectra (the spectra obtained for the un-colored suspension). The results presented in table 4 show the sample TiO_2-T K400 as the best photocatalyst what correlates well with presence of anatase and its crystallite size (see table 2).

3.3.5 Scanning electron microscopy

The morphology of the selected TiO_2 samples prepared using syntheses No.1 – No.3 was studied using SEM (Philips XL 30). To make the samples conductive the samples were sputtered with an Au/Pd film. SEM images were obtained using a secondary electron detector (SE) and are presented in Fig. 29.

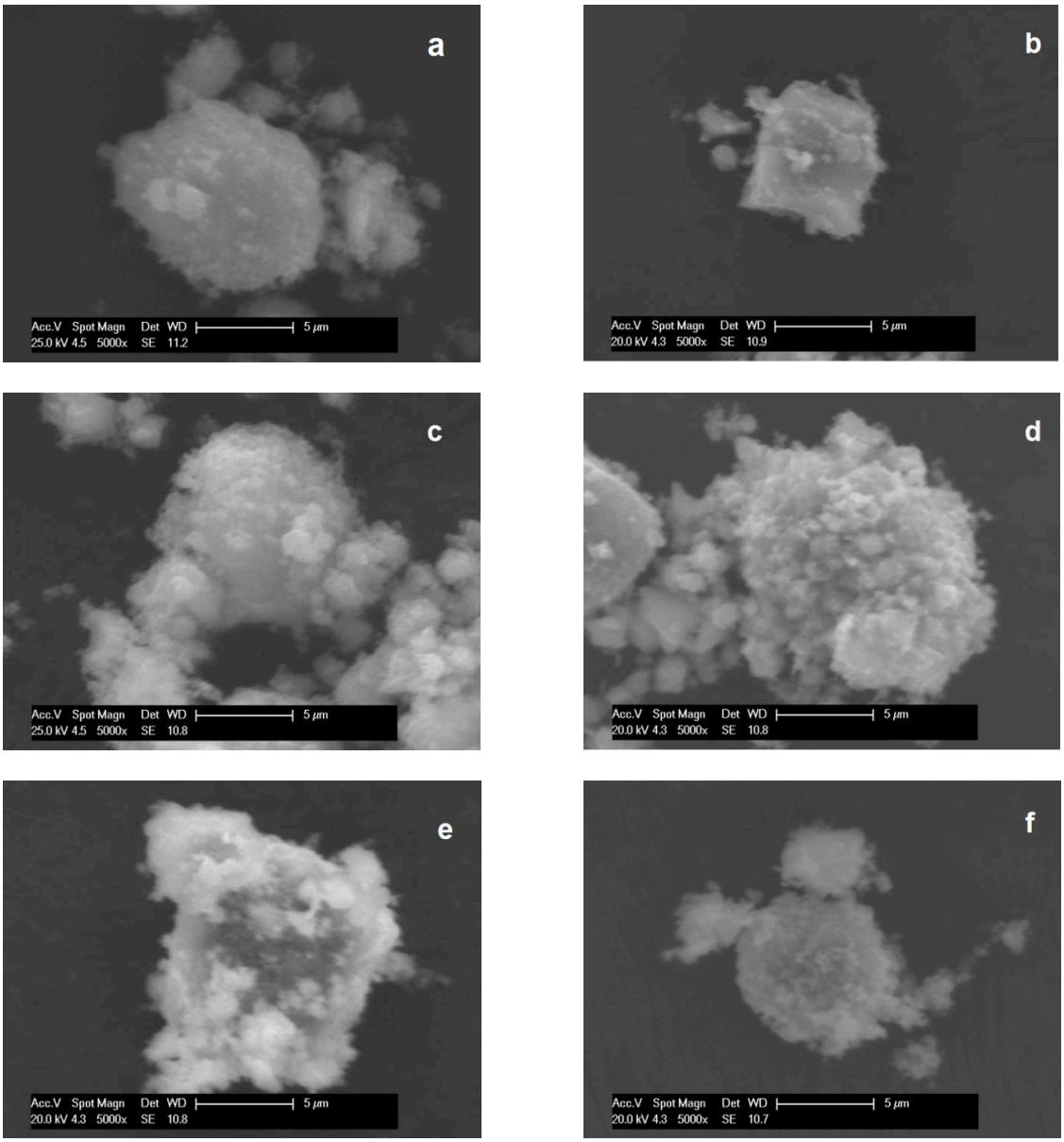

Fig. 29 SEM images of sample: (a) TiO_2 105, (b) TiO_2 K400, (c) TiO_2-T 105, (d) TiO_2-T K400, (e) TiO_2-MZ 105, and (f) TiO_2-MZ K400.

The first two images in Fig. 29 were acquired at different accelerating voltages. The filament had become unstable during the measurement session and the voltage had to be lowered. Otherwise the measurement proceeded without problems.

As can be seen from the Figures 29d and 29e, all of the particles are agglomerates covered with smaller particles. The size of the particles varied for each sample, uniform particle size distribution was not observed. The morphology of the TiO_2 samples is closely similar and the size of the agglomerates was in the order of micrometers. The effect of calcination on agglomerate size was not observed.

The elemental composition of the samples was acquired by the Energy-dispersive X-ray spectroscopy (EDX) and revealed the presence of titanium and sodium at all of the samples, the presence of sulphur was not verified. Sodium content determined using EDX analysis performed at the selected area of the imaged samples is shown in Tab. 5. The presence of sodium impurities in sample was reported to support phase transition from anatase to rutile and formation of sodium hexa-titanate phases e.g. by Zita et. al. [37].

Tab. 5 Sodium content in the samples in wt%.

Sample	Sodium content
TiO_2 105	8.2
TiO_2-T 105	5.2
TiO_2-MZ 105	10.9
TiO_2 K400	6.5
TiO_2-T K400	5.7
TiO_2-MZ K400	9.0

3.3.6 Physisorption

The physisorption of the selected samples was determined using the nitrogen adsorption-desorption measurements at - 198 °C. The measurement was performed using the Sorptomatic 1990 instrument (Thermo Fisher Scientific Inc., Italy) shown in Fig. 30. Prior to the nitrogen physisorption measurements, the samples were degassed at temperature 110 °C for 12 h under vacuum lower than 1 Pa. The degassing was applied in order to remove physisorbed water.

Fig. 30 Photo of Sorptomatic 1990, Thermo Fisher Scientific.

The specific surface area was calculated according to the classical Brunauer–Emmett–Teller (BET) theory for the p/p_0 range 0.05-0.25 and is marked as S_{BET} (m^2/g) [33, 38]. The net pore volume, V_{net} (mm^3_{liq}/g) was determined from the nitrogen adsorption isotherm at maximum p/p_0 (~0.9995). The data gathered from the SSA measurement are summarised in Tab. 6.

Tab. 6 The overview of data gathered from the SSA measurement.

sample	isotherm type	porosity	S_{BET}	$V_{net}^{\bullet}$
TiO_2 K400	IV	mesoporous	59.3	180
TiO_2-T K400	I + IV	micro-mesoporous	97.8$^{\#}$	238
TiO_2-MZ K400	II	meso-macroporous	14.1	87

Comparing the data in Tab 6 the sample TiO_2-T K400 shows significantly larger specific surface area (97.8 m^2/g) than the other samples. The net pore volume corresponds well with the values of specific surface area.

The S_{BET} value of the sample TiO_2-T K400 is slightly overestimated due to the presence of small amount of micropores. The stated net pore volume covers only the volume of pores with diameter smaller than 80 nm. The adsorption–desorption isotherms are shown in Fig. 31 Fig. 33 below. The adsorption isotherms are presented in black color and desorption isotherms are in red color.

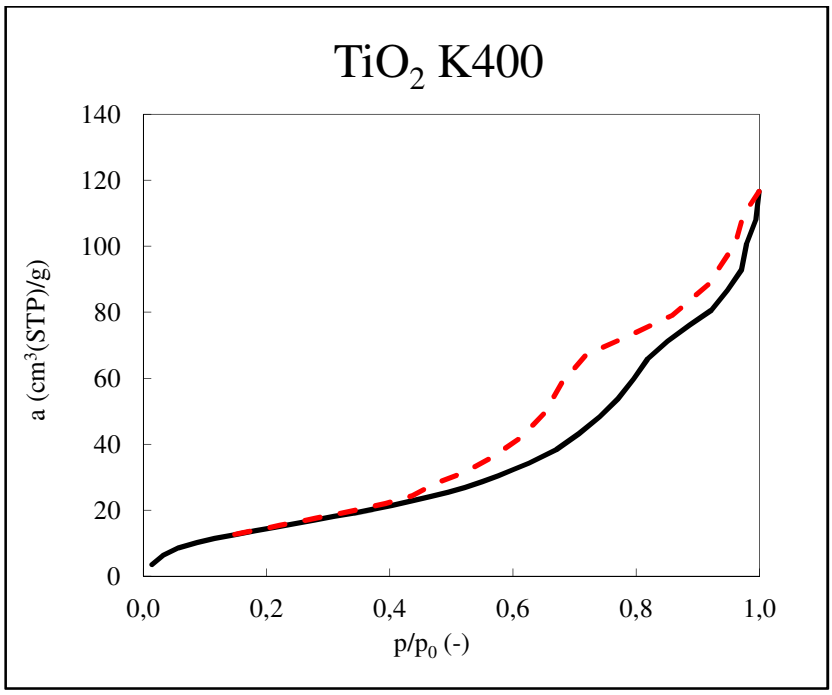

Fig. 31 Adsorption (in black color) - desorption (in red color) isotherm for sampleTiO_2 K400.

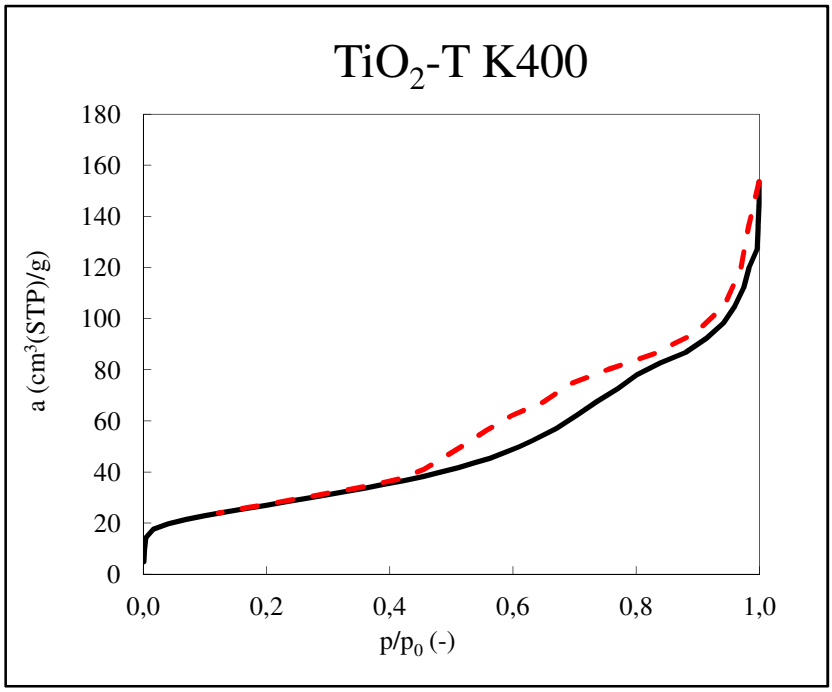

Fig. 32 Adsorption (in black color) - desorption (in red color) isotherm for sample TiO_2-T K400.

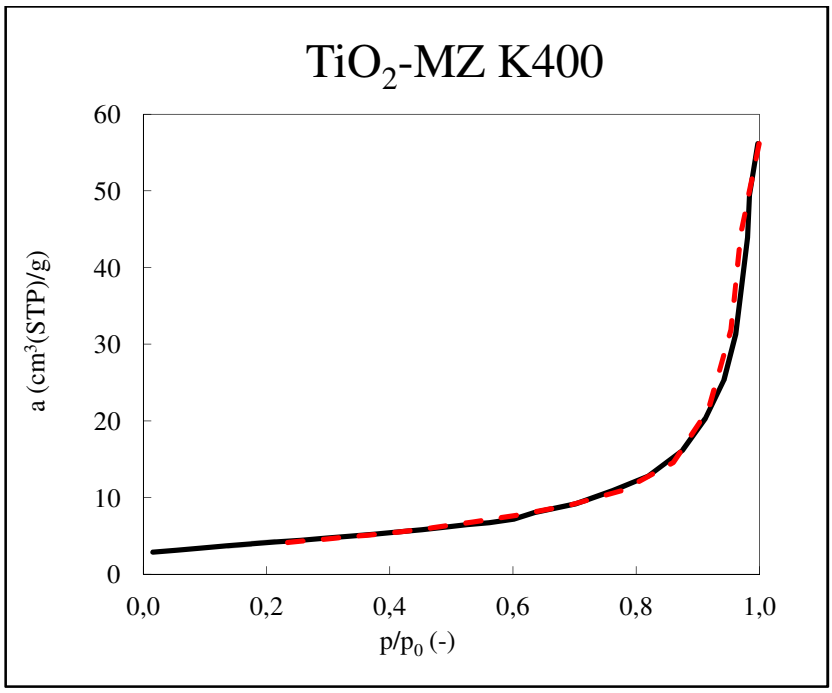

Fig. 33 Adsorption (in black color) - desorption (in red color) isotherm for sample TiO_2-MZ K400.

The porosity of the samples was evaluated from the registered isotherms. The isotherms in Fig. 31 represent isotherm of IV type which is typical for mesoporous materials. In Fig. 32 is isotherm combining I and IV type. This combination of isotherms describes micro-mesoporous material. Hysteresis loop between adsorption and desorption branch is clearly apparent in Fig. 31 and Fig. 32 is, in Fig. 33 the adsorption and desorption isotherm overlaps and no hysteresis loop is visible. Isotherm in Fig. 33 is the type II and is typical for meso-macroporous materials.

The absence of hysteresis loop observed for sample TiO_2-MZ K400 means that the adsorbed and desorbed volume of adsorbate is identical and there is no retention in the pores. The isotherm in Fig. 33 is typical for meso-macroporous materials which have easily accessible pores with shape that does not prevent desorption e.g. cylindrical shape. With respect to values of specific surface area the sample TiO_2-T K400 should exhibit the best photocatalytic activity.

4 Conclusion

Based on the knowledge gathered from literature research, three synthesis methods for TiO_2 using titanyl sulphate were proposed and tested. Photocatalytic active TiO_2 was successfully prepared from each of the methods. The products were characterized using X–ray diffraction, sulphur analysis, photocatalytic activity measurement, thermal analysis, scanning electron microscopy and physisorption.

The photocatalytic activity was evaluated according to Precheza a.s. internal method for powder samples using aquatic suspension of sample and model dye subjected to UV irradiation. The best photodegradation activity show the samples prepared by synthesis No.2. The photocatalytic activity was positively affected by calcination of the TiO_2 samples obtained from all of the tested syntheses. The samples calcinated at 400 °C for 1 h show the highest photodegradation activity.

The sulphur content at the samples was determined by combustion method. The measured content of the sulphur revealed the fact, that the sulphate ions cannot be decreased below 1 wt% by washing even with high volume of water (10 L).

The sodium content at selected samples was determined by EDX analysis. The sodium content was surprisingly high and the values differed among the syntheses. The sodium content ranged from 5wt % to 10 wt% in samples prepared using synthesis No.2 and synthesis No.3, respectively. Although sodium hydroxide (NaOH) is more ecologically suitable neutralization agent than ammonium hydroxide (NH_4OH), it serves as a source of sodium cations Na^+ ions that may have negative effect on TiO_2 photocatalytic activity whereas the data obtained in experimental section support this theory.

The water content was determined by thermogravimetric analysis of the samples previously dried at 105 °C. The values ranged from 10 wt% in sample from synthesis No.2 to 15 wt% in sample from synthesis No.3.

The phase composition of the samples was determined by X–ray diffraction method. Prior to heat treatment the prepared samples show amorphous character. The heat treatment of the samples resulted in increase in the crystallite size. The presence of anatase, rutile and hexa-titanate ($Na_2Ti_6O_{13}$) phases in samples was detected. The anatase phase was identified in samples from all three syntheses. The anatase phase transformed to rutile phase in samples from syntheses No.1 and No.2 after their calcination at 800 °C for 1 h. The sodium hexa-titanate ($Na_2Ti_6O_{13}$) was observed in samples from all three syntheses calcined at 800 °C. The

phase transition of anatase phase to rutile phase and development of sodium hexa-titanate ($Na_2Ti_6O_{13}$) were linked to decrease in photoactivity.

The specific surface area and net pore volume were evaluated by physisorption. The selected sample from the synthesis No.2 calcined at 400 °C had almost two times higher specific surface area compared to sample from synthesis No.1 and almost seven times higher compared to sample from synthesis No.3. The porosity of the selected samples was determined from the adsorption-desorption isotherms. The presence of micropores was detected in sample obtained from synthesis No.2 calcined at 400 °C (TiO_2-T K400). The positive effect of the size of the specific surface area on the photodegradation activity of the prepared samples was shown.

The morphology of the samples was determined using scanning electron microscopy and using this method the presence of large agglomerates in micrometer dimensions was detected.

The aims of the diploma thesis were successfully accomplished. All three preparation methods produced photoactive TiO_2. The best photocatalytic activity showed sample TiO_2-T K400 prepared by method No.2 and calcined at 400 °C.

5 Acknowledgment

The diploma thesis has been elaborated in the framework of the Nanotechnology – the basis for international cooperation project, reg. No.**CZ.1.07/2.3.00/20.0074,** supported by Operational Programme 'Education for competitiveness' funded by Structural Funds of the European Union and the state budget of the Czech Republic.

I would like to thank to my supervisor doc. Ing. Vlastimil Matějka, Ph.D. for helpful consultations of my diploma thesis provided beyond regular classes and to Ing. Pavel Kovář as a consultant from industrial partner Precheza a.s. Further, I would like to thank Ing. Lenka Matějová, Ph.D., Ing. Soňa Študentová and Ing. Jiřina Vontorová, Ph.D.

6 Literature

[1] GOULD, P.; Nanomaterials face control measures. *Nanotoday*. 2006, vol. 1, no 2, p. 34-39.

[2] Sigma-Aldrich, Inc: Support. [online]. © 2013 [cit. 2013-05-01]. Available from: http://www.sigmaaldrich.com/catalog/AdvancedSearchPage.do

[3] VILÍMOVÁ, P; *Dopace kompozitu kaolinit/TiO_2 dusíkem*. Ostrava, 2012. Bakalářská práce. Vysoká škola báňská - Technická univerzita Ostrava. Vedoucí práce Ing. Matějka Vlastimil, Ph.D.

[4] CARP, O.; HUISMAN, C., L; RELLER, A.; Photoinduced reactivity of titanium dioxide. *Progress in Solid State Chemistry*. 2004, vol.32, no.1-2, p.33-177.

[5] VALENCIA, S; MARÍN, J., G.; RESTREPO, G. Study of the Bandgap of Synthesized Titanium Dioxide Nanoparticules Using the Sol-Gel Method and a Hydrothermal Treatment. *The Open Materials Science Journal.* 2010, vol.4, p. 9-14.

[6] KHATAEE, A.; MANSOORI, G., A.; Nanostructured Titanium dioxide materials, properties, preparation and applications, Singapore: World scientific publishing Co. Pte. Ltd, 2012, ISBN-13: 9789814374729.

[7] ŘEPKA, V.; POSSIBILITIES OF TITANIUM ORE DRESSING, *Sborník vědeckých prací Vysoké školy báňské – Technické univerzity Ostrava Řada hornicko-geologická Volume LII*, Vydala Vysoká škola báňská – Technická univerzita Ostrava, 2006, No.2, p. 21-29, ISSN 0474-8476.

[8] KUNDRÁT, L. *Studium rozkladu ilmenitu při sulfátovém způsobu výroby titanové běloby*. Pardubice, 2003. Diplomová práce. Univerzita Pardubice, Fakulta chemicko – technologická, Katedra anorganické technologie.

[9] BUXBAUM, G. *Frontmatter, in Industrial Inorganic Pigments*, Weinheim, Germany: Wiley-VCH Verlag GmbH, 2007, 2ed, ISBN: 978-3-527-30363-2, Available from: http://onlinelibrary.wiley.com/book/10.1002/9783527612116;jsessionid=DB40AFB1D892EC4B90B85820415AD685.d04t03

[10] KANEKO, M.; OKURA, I.; *Photocatalysis: science and technology*. Verlag Berlin Heidelberg New York: Springer, 2002. ISBN: 3-540-43473-9.

[11] LEARY, R.; WESTWOOD, A.; Review Carbonaceous nanomaterials for the enhancement of TiO_2 Photocatalysis. *Carbon*., 2011, vol. 49 , p. 741 – 772.

[12] HAN, F.; KAMBALA V., S., R.; SRINIVASAN, M.; et al.; Tailored titanium dioxide photocatalysts for the degradation of organic dyes in wastewater treatment: A review. *Applied Catalysis A: General*, 2009, vol.359, p. 25–40.

[13] GOMES DA SILVA, C., S., C.; *Synthesis, Spectroscopy and Characterization of Titanium Dioxide Based Photocatalysts for the Degradative Oxidation of Organic Pollutants*; Portugal, 2008. PhD thesis University of Porto, Faculty of Engineering. Available from: http://repositorio-aberto.up.pt/bitstream/10216/11536/2/Texto%20integral.pdf

[14] AHMED, S.; RASUL, M.G.; BROWN, R.; HASHIB, M., A.; Influence of parameters on the heterogeneous photocatalytic degradation of pesticides and phenolic contaminants in wastewater: A short review. *Journal of Environmental Management*, 2011, vol. 92, p. 311-330.

[15] BARTOVSKÁ, L.; ŠIŠKOVÁ, M.; *Fyzikální chemie povrchů a koloidních soustav*. Praha: Vysoká škola chemicko-technologická, 2010. 6. Ed, ISBN 978-80-7080-745-3.

[16] VOJUCKIJ, S; *Kurz koloidní chemie*. Přeložili: KARPENKO, V., ŠOBR, J.; Praha: SNTL, 1984, 9745. publication.

[17] Http://www.ncbi.nlm.nih.gov/guide/: PubChem Compound. [online]. 2009-9-28 [cit.2013-05-01].
Available from: http://pubchem.ncbi.nlm.nih.gov/summary/summary.cgi?cid=61684

[18] ROCHE et al. *Sulfate process*. US Patent 8273322. 2012-9-25. Available from: https://docs.google.com/viewer?url=patentimages.storage.googleapis.com/pdfs/

US8273322.pdf

[19] GRZMIL, B.U.; GRELA, D.; KIC, B.; Hydrolysis of titanium sulphate compounds. *Chemical Papers*. 2008, vol. 62, no 1, p. 18-25.

[20] MECKLENBURG, WERNER. *Production of Titanium dioxide*. US Patent 1758528. 1930-5-13. Available from: https://docs.google.com/viewer?url=www.google.com/

patents/US1758528.pdf

[21] BLUMENFELD, JOSEPH. *Production of Titanium dioxide*. US Patent 1795467. 1931-3-10. Available from https://docs.google.com/viewer?url=www.google.com/patents/

US1795467 .pdf

[22] GRZMIL, B.U.; GRELA, D.; KIC, B.; PODSIADLY, M.; The influence of admixtures on the course of hydrolysis of titanyl sulfate. *Polish Journal of Chemical Technology*. 2008, vol. 10, no 3, p. 4-12.

[23] GRZMIL, B.U.; GRELA, D.; KIC, B.; Effects of processing parameters on hydrolysis of $TiOSO_4$. *Polish Journal of Chemical Technology*. 2009, vol. 11, no 3, p. 15-21.

[24] VALVODA, V. *Rentgenografické difrakční metody*. 1st edition. Praha: Univerzita Karlova, 1983.

[25] VALVODA, V. *Rentgenová strukturní analýza*. 1st edition. Praha: Státní pedagogické nakladatelství, 1982.

[26] STUART, H., B.; Infrared Spectroscopy: Fundamentals and Applications. John Wiley & Sons, Ltd, 2005. ISBN: 978-0-470-85428-0.

[27] WORKMAN, J.; SPRINGSTEEN, A.; *Solar Transmittance in Applied Spectroscopy: A Compact Reference for Practitioners.* 1st edition Massachusetts: Academic Press, 1998.

[28] VIK, M.; *Základy měření barevnosti I.díl*, 1st edition Liberec: Technická univerzita v Liberci, 1995.

[29] BŘEZINA, F.; *Stereochemie a některé fyzikálně chemické metody studia anorganických látek*. 3st edition, Olomouc: Přírodovědná fakulta, Univerzita Palackého, 1994.

[30] CHARSLEY, E., L.; WARRINGTON, S., B.; Thermal analysis – Techniques & Applications. Thermal Analysis Consultancy Service, Leeds: Leeds Metropolitan University, 1992, ISBN: 0-85186-375-2.

[31] AMELINCKX, S.; VAN DYCK, D.; VAN LANDUYT, J.; VAN TENDELOO, G.; Electron microscopy Principles and Fundamentals, Wiley-VCH. 1st edition, 1997. ISBN 3-527-29479-1.

[32] SCHNEIDER, P.; Textura porézních látek, Učební text pro doktorské studium, Ústav chemických procesů AV ČR, Praha, 2002.

[33] GREGG, S., J.; SING, K., S., W.; *Adsorption. Surface Area and Porosity*. New York: Academic Press, 2st edition, 1982. ISBN-13: 978-0123009562.

[34] DONOHUE, M., D.; ARANOVICH, G., L.; Classification of Gibbs adsorption isotherms. *Advances in Colloid and Interface Science*, 1998, vol. 76-77, p.137-152.

[35] SIVAKUMAR, S.; KRISHNA PILLAI P.; MUKUNDAN, P.; WARRIER, K.G.K. Sol–gel synthesis of nanosized anatase from titanyl sulfate. *Materials Letters*, 2002, vol. 57, p. 330–335.

[36] SCHERRER, P.; Estimation of the previous and internal structure of colloidal particles by means of roentgen rays, *Nachr. Ges. Wiss. Gottingen*, 1918, p. 96–100.

[37] ZITA, J.; MAIXNER, J.; KRÝSA. J.; Multilayer TiO_2/SiO_2 thin sol-gel films. Effect of calcination temperature and Na^+ diffusion. *Journal of Photochemistry and Photobiology A:Chemistry 216,* 2010, vol.216, p.194-200

[38] BRUNAUER, S.; EMMETT, P., H.; TELLER, E.; Adsorption of gases in multimolecular layers, *J. Am. Chem. Soc.* 1938.vol. 60, p.309-319.

7 Attachments

Titanyl sulphate card 81-1567 from the database PDF 2 Release 2012.